ARTTU HEININEN
MODELLING AND SIMULATION OF AN AIRCRAFT MAIN LANDING GEAR SHOCK ABSORBER
Master of Science Thesis

TIIVISTELMÄ

Jokaisen perinteisen lentokoneen päälaskutelineissä on iskunvaimennin, jonka tehtävä on ottaa laskeutumisesta aiheutuva isku vastaan, absorboida se ja dissipoida kineettinen energia. Tässä työssä tutkittiin taisteluhävittäjän öljypneumaattisen joustimen mallinnusta ja simulointia. Iskunvaimentimen toimintaa hallitsevat yhtälöt on esitetty, joihin sisältyvät muun muassa kitkan, kaasujousen ja vaimennuksen käyttäytyminen.

Malli on validoitu vertaamalla simulointituloksia referenssimittauksilla saatuihin tuloksiin. Validoinnin aikana havaittiin korkeita kitkatasoja. Referenssidataa oli saatavilla staattisesta testipenkistä, dynaamisesta testijärjestelmästä sekä oikeasta laskeutumisesta. Työssä esitetty malli tuotti tuloksia, jotka olivat lähellä mitattuja arvoja. Lisäksi suoritettiin simulointeja vaihtelemalla kaasun ja nesteen suhdetta sekä lämpötilaa. Kaasun ja nesteen suhteen merkittävä muutos saattaa aiheuttaa päälaskutelineen viallisen toiminnan, mutta asian todentaminen vaatii lisätutkimusta. Lämpötilaa vaihdeltiin kahdella tapaa. Ensin alkulämpötilaa vaihtamalla ja sitten lämmittämällä tai jäähdyttämällä iskunvaimenninta simuloinnin aikana. Jos iskunvaimentimen täyttölämpötilan ja ulkolämpötilan välillä on lämpötilaero, paine iskunvaimentimen sisällä kasvaa tai pienenee, riippuen lämmitetäänkö vai jäähdytetäänkö iskunvaimenninta, mikä voi aiheuttaa viallisen toiminnan. Mallia voidaan käyttää työkaluna kunnonvalvonnan kehittämisessä sekä vikatilojen tutkimisessa. Suunnitteilla on myös uusi mittalaite, jonka suunnitteluvaiheessa mallia voidaan käyttää hyödyksi.

Työssä esitetty malli approksimoi todellisen iskunvaimentimen kaasujousen sekä kuristustapin toimintaa hyväksyttävällä tarkkuudella, mutta ei ota huomioon mahdollisia muodonmuutoksia, jotka voivat syntyä korkeiden paineiden takia. Parannusehdotuksia on esitetty sekä pohdittu ja tavoitteena on, että nämä esitetyt parannusehdotukset liitetään malliin lähitulevaisuudessa. Myöhemmin tavoitteena on liittää paranneltu malli suurempaan päälaskutelineen malliin, jonka avulla laskeutumista ja siihen liittyviä ilmiöitä voidaan tarkastella kokonaisuutena.

ABSTRACT

TAMPERE UNIVERSITY OF TECHNOLOGY
Master's Degree Programme in Mechanical Engineering
HEININEN, ARTTU: Modelling and simulation of an aircraft main landing gear shock absorber
Master of Science Thesis, 53 pages, 3 Appendix pages
September 2015
Major: Fluid dynamics
Examiner: Professor Kari T. Koskinen
Keywords: Amesim, modelling, simulation, aircraft, shock absorber, landing gear

Every traditional aircraft has a shock absorber in its main landing gear. A shock absorber takes the brunt of the shock imparted to the landing gear, absorbs it and dissipates the kinetic energy. This thesis is based on the construction of a realistic analytical model of an oleo-pneumatic shock absorber for a combat aircraft. The governing equations presented here include the effects of friction, gas spring and damping, among other things.

The model was validated with a wide range of reference data, which revealed exceptionally high friction levels detected during the validation process. The reference data consists of measurements from a static test bench, a dynamic test system and an actual aircraft landing, and the corresponding simulations are presented in this thesis. The results of the simulations closely match the measured data. The effects of variations in the gas-liquid ratio and temperature on the pressure behaviour inside the shock absorber were simulated. If the gas-liquid ratio is distorted, the damping ability of the shock absorber is diminished, which may lead to faulty operation of the landing gear. Temperature variation was examined in two ways, firstly by varying the initial temperature and secondly, by heating and cooling the shock absorber. Filling the shock absorber in conditions which differ from the environment in which the aircraft will operate causes the pressure to decrease or increase, depending on whether the shock absorber is cooled or heated. The utilization of simulations as a tool in condition monitoring and fault detection is discussed, and as a result of that a new measuring instrument is proposed, whose design can be facilitated with this simulation model.

Although the model presented in this thesis is not complete, it adequately mirrors the behaviour of the gas spring and the metering bin. However, the model does not include the deformations caused by high pressures. A number of possible improvements to the model are presented and discussed. In its present form, the load-stroke behaviour of the model is close to the real shock absorber, and the model can be used to analyse the forces and pressures generated by different shocks. Future work will involve improving the model and incorporation of the model into a larger main landing gear model so that a comprehensive investigation of the dynamics of an aircraft landing can be performed.

PREFACE

I would like to express my gratitude to my supervisors Professor Kari T. Koskinen and M.Sc. Jussi Aaltonen for their guidance and advice during the process of working on this thesis. I would also like to thank the Department of Mechanical Engineering and Industrial Systems and the Finnish air force for giving me this opportunity to carry out this research.

I am grateful to B.Sc. Juha Huitula from the FDF Logistics Command for the information he provided. I would also like to express my gratitude to all the teaching personnel, who have taught me during my studies here at Tampere University of Technology.

Tampere, November 24, 2015

_____

Arttu Heininen

CONTENTS

LIST OF SYMBOLS

Greek symbols:

α	Volumetric expansion coefficient	[1/K]
α_T	Thermal diffusivity	[m^2/s]
α_V	Volumetric expansion coefficient	[1/K]
β	Fluid bulk modulus	[Pa]
Γ	Polytropic index	
δQ	Heat exchange with surroundings	[W]
Δp	Pressure difference	[Pa]
λ	Flow number	
λ_{crit}	Critical flow number	
θ	Angle of inclination	[rad]
μ	Dynamic viscosity	[Pa·s]
μ_c	Coulomb friction coefficient	
v	Kinematic viscosity	[m^2/s]
ρ	Density	[kg/m^3]
ω	Pitzer's acentric factor	

Latin symbols:

a	Attractive term	[(N·m)/kg]
a_1	Inner mass acceleration	[m/s^2]
a_2	Envelope acceleration	[m/s^2]
A	Orifice cross section	[m^2]
A_{HP}	High pressure chamber cross-sectional area	[m^2]
A_{mp}	Metering pin cross-sectional area	[m^2]
A_S	Seal outer surface	[m^2]
A_{PF}	Effective piston ring area	[m^2]
A_{ph}	Annulus area of the primary piston head	[m^2]
b	Covolume	[m^3/kg]
c_p	Specific heat capacity	[J/(K·kg)]
c_q	Flow coefficient	

c_q	Maximum flow coefficient	
C_P	Specific heat of the fluid	[J/(kg·K)]
d_c	Clearance between an envelope and a piston	[m]
d_p	External piston diameter	[m]
dh	Heat flow rate	[W]
dp	Piston diameter	[m]
dr	Piston rod diameter	[m]
dm	Mass flow rate	[kg/s]
dmh	Incoming enthalpy flow rate	[W]
dmh_{down}	Downstream enthalpy flow rate	[W]
dmh_{up}	Upstream enthalpy flow rate	[W]
dv	Zero velocity interval	[m/s]
D_P	External piston diameter	[m]
Db_{max}	Higher limit contact damping coefficient	[N/(m·s)]
Db_{min}	Lower limit contact damping coefficient	[N/(m·s)]
F_{dry}	Dry friction force	[N]
F_{max}	Higher limit contact force	[N]
F_{max2}	Higher limit contact force between the envelope and the fixed reference	[N]
F_{max3}	Higher limit contact force between the inner mass and the fixed reference	[N]
F_{min}	Lower limit contact force	[N]
F_{min2}	Lower limit contact force between the envelope and the fixed reference	[N]
F_{min3}	Lower limit contact force between the inner mass and the fixed reference	[N]
F_1	Piston force at the positive port	[N]
F_2	Piston force at the negative port	[N]
F_{added}	Added force	[N]
F_{sum1}	Force on the inner mass	[N]
F_{sum2}	Force on the envelope	[N]
F_{exti}	Force acting on port i	[N]
F_C	Coulomb friction force	[N]
F_{FP}	Piston friction force	[N]
F_N	Normal force	[N]

F_S	Stiction force	[N]
F_V	Viscous friction force	[N]
F_V	Coefficient of viscous friction	[N/(m·s)]
F^+	Envelope friction force	[N]
F^-	Piston friction force	[N]
g	Gravitational acceleration	[m/s²]
h	Specific enthalpy of the volume	[J/kg]
k	Thermal conductivity	[W/(m·K)]
K	Constant	
Kb_{max}	Higher limit stiffness	[N/m]
Kb_{min}	Lower limit stiffness	[N/m]
K_H	Henry's law constant	[Pa]
l_c	Contact length	[m]
L	Seal ring axial length	[m]
m	Mass of the fluid	[kg]
m_{sa}	Mass of the shock absorber	[kg]
m_1	Mass of the inner mass	[kg]
m_2	Mass of the envelope	[kg]
p	Pressure	[Pa]
p_{init}	Initial pressure	[Pa]
p_{ns}	Normal service pressure	[Pa]
p_{up}	Upstream pressure	[Pa]
P	Pressure	[Pa]
P_{atm}	Atmospheric pressure	[Pa]
P_{crit}	Critical pressure	[Pa]
P_P	Piston pressure	[Pa]
Pd_{max}	Higher limit penetration for full damping	[m]
Pd_{min}	Lower limit penetration for full damping	[m]
Q	Volumetric flow rate	[m³/s]
r	Specific gas constant	[J/(kg·K)]
r_c	Radial clearance	[m]
R_{visc1}	Viscous friction between the piston and the envelope	[N/(m·s)]
R_{visc2}	Viscous friction between the envelope and the fixed reference	[N/(m·s)]
T	Temperature of the volume	[K]

T_{crit}	Critical temperature	[K]
T_{up}	Upstream temperature	[K]
v	Relative velocity	[m/s]
v_s	Specific volume of the fluid	[m³/kg]
v_s	Stribeck velocity	[m/s]
v^+	Envelope velocity	[m/s]
v^-	Piston velocity	[m/s]
V	Volume	[m³]
V_2	Envelope velocity	[m/s]
V_{rel}	Relative velocity	[m/s]
W_1	Windage friction between the piston and the envelope	[N/(m·s)²]
W_2	Windage friction between the envelope and the fixed reference	[N/(m·s)²]
x	Gas content	[(N·m)/kg]
X_{max}	Higher displacement limit	[m]
X_{min}	Lower displacement limit	[m]
X_{rel}	Relative displacement	[m]
X_{ref}	Inertial reference position	[m]
Z	Compressibility factor	

LIST OF FIGURES

1. INTRODUCTION

Every traditional aircraft has a shock absorber in the *main landing gear* (MLG) assembly. The shock absorber takes the brunt of the shock imparted to the landing gear, absorbs it and dissipates the kinetic energy. The most common shock absorber in retractable landing gear assemblies is the *oleo-pneumatic shock absorber* [1, p. 168]. This is a two-chamber telescopic hydraulic cylinder with sealed ends. The lower chamber is filled with hydraulic fluid and the upper chamber contains compressed gas, usually dry air or nitrogen. When the shock absorber is under an external load, the fluid flows from the lower chamber to the upper chamber through an orifice which dampens the motion. The fluid flow rate is controlled by a *metering pin* with a variable diameter to achieve the designed load-stroke relation for the shock absorber. The compressed gas in the upper chamber acts as a spring under the load and cushions the impact as the pressure rises. A generic oleo-pneumatic shock absorber and its main components are shown in Figure 1.1, where the hydraulic fluid is shown in red and the gas in white.

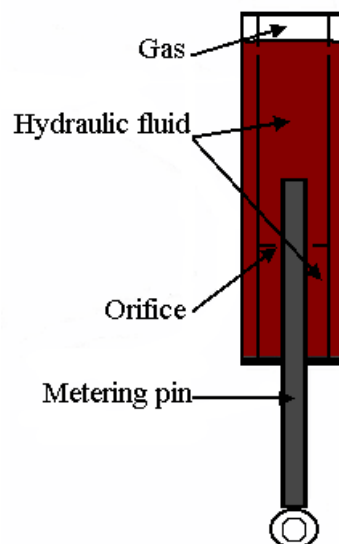***Figure 1.1.*** *A generic oleo-pneumatic shock absorber.*

This work was carried out at Tampere University of Technology in the department of Mechanical Engineering and Industrial Systems as a part of a project commissioned by the Finnish Air Force (FiAF). The objective of this thesis is to understand the physical phenomena occurring inside the shock absorber using modelling and simulation as a re-

search method. To achieve this objective, a realistic analytical simulation model of a combat aircraft's modified oleo-pneumatic shock absorber, (hereinafter referred to as an 'oleo-pneumatic shock absorber' or simply a 'shock absorber') was built, for which the governing equations are presented here. The thesis discusses utilization of the model as a tool in condition monitoring and fault detection. A simulation model is rarely a perfect copy of the object that it is modelling, and therefore the limitations of the model and suggestions for possible improvements are also discussed.

The shock absorber differs from a conventional oleo-pneumatic shock absorber by having a high pressure chamber added to it. This chamber is filled only with gas and it enables the shock absorber to absorb greater impact loads than a conventional oleo-pneumatic shock absorber of the same size. Higher impact loads mean higher sink speeds, such as those which occur, for example, when landing on an aircraft carrier. A modified oleo-pneumatic absorber for a combat jet is shown in Figure 1.2.

The modelling and simulation were done using a commercial multi-domain system simulation software LMS Imagine.Lab AMEsim revision 13. Regarding the literature review, simulation is a common tool in both the aircraft and automotive industries, and telescopic hydraulic shock absorbers are the most widely used shock absorbers in the automotive industry [2, p. 9], so there are a plethora of research papers and articles about the modelling and simulation of shock absorbers. Therefore, due to the limited scope of this thesis, only the most relevant and interesting ones are discussed in this work.

One of the first published oleo-pneumatic shock absorber analyses was made by Hadekel [3]. Milwitzky and Cook carried out an analysis on landing gear behaviour [4]. Yadav and Ramamoorthy incorporated the effects of non-linearities in air spring and oleo damping forces at touchdown [5]. Daniels validated a simulation model of an A6-Intruder attack aircraft with experimental data [6] and Horta, Daugherty and Martinson extended this by incorporating active controls [7]. Reineh modelled and simulated a racing car shock absorber using Amesim in her Master's Thesis [8].

The following chapter discusses the sources used from the literature and the third chapter presents the shock absorber assembly and the simulation model of the shock absorber, as well as the equations governing the principles of the shock absorber operation. In the fourth chapter, the model is validated with reference measurement data provided by FiAF. Chapter 5 presents and analyses the simulations results. The sixth chapter discusses the limitations of the model and possible improvements which could be made, and the thesis finishes with the main conclusions which can be drawn from this research.
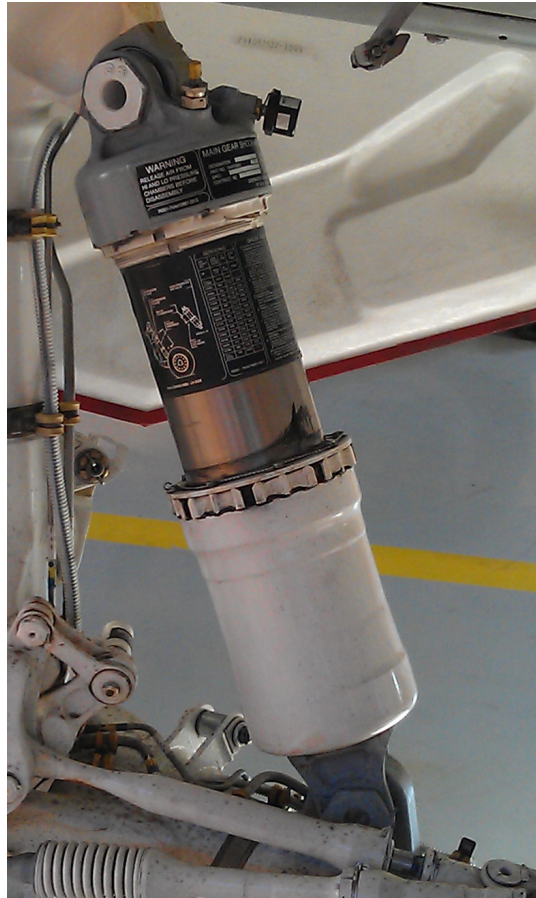
Figure 1.2. *A modified oleo-pneumatic shock absorber from a combat aircraft.*

2. STATE OF THE ART

As stated above, because shock absorbers are such a common device, particularly in the car industry, they have been studied with simulations for quite some time. Simulations reduce the amount of empirical testing required, and can therefore reduce the costs and time expended during the design phase of a product. They can be used to analyse the behaviour of a shock absorber during landing and/or taxiing and can also simulate situations that are outside of the shock absorber's normal service range. Simulation provides a safe and inexpensive way to experiment with the system which is under simulation [9, p. 15].

Combat aircraft are used in extreme conditions and, unlike commercial aircraft, the main landing gear in a combat aircraft has to be individually tailored for the aircraft as there is only minimal room for the landing gear in the fuselage [10, p. 437]. Naturally, this also applies to the shock absorber, as it is part of the landing gear assembly. Each type of combat aircraft is designed for a specific task, so they vary in weight and shape, which means that each type of combat aircraft requires its own, unique simulation model to achieve accurate results. However, building a new model has to be done with the utmost care as the accuracy of the simulation measurements is entirely dependent on the quality of the model [9, p. 15]. This chapter discusses some previous oleo-pneumatic shock absorber analyses.

2.1 Literature review

The development of shock absorber analyses dates back to at least the 1940's, when Hadekel presented his oleo-pneumatic shock absorber calculations [3]. He stated that the oleo- pneumatic shock absorber is the most effective type of suspension system [3, p. 71]. This was later confirmed by Currey, who stated that oleo-pneumatic shock absorbers have the highest efficiencies and the best energy dissipation of all shock absorber types [10, p. 75]. Currey also stated that the load-stroke curve could be calculated using iso-thermal compression of the gas during ground operation and a polytropic compression during landing [10, p. 100]. Currey also suggested that the polytropic index of a polytropic process is greater when nitrogen and oil are in separate volumes, than when they are in one volume, as mixing them causes a loss of adiabatic compression because the gas is cooled by the oil.

Milwitzky and Cook [4] presented a theoretical study of the kinematics of a conventional oleo-pneumatic shock absorber during landing. They presented the equations of

motion and a system for a single-degree-of-freedom, which was validated with experimental drop test data. The compression was modelled as a polytropic process. The main conclusions were that the discharge coefficient of the orifice has a notable effect on the calculated behaviour of the shock absorber, while the air springing plays only a minor role during most of the impact [4, p. 32].

Yadav and Ramamoorthy analysed the nonlinear behaviour of a landing gear assembly at touchdown [5]. They carried out a simulation using a heavy-pitch model they had created for a small fighter-trainer aircraft. They observed that the damping effect was increased when the orifice discharge coeffiecient was decreased. They also suggested that the use of active control in a shock absorber would improve the landing gear's performance [5, p. 682].

Daniels modelled and simulated an A6-Intruder naval attack aircraft landing gear [6]. Among other things Daniels' model included nonlinear effects such as polytropic compression, velocity squared damping, a geometrically governed model for the discharge coefficient and the stick-slip effect. The model was validated using static and dynamic data. The results were accurate, and simulation was recognised as being a powerful tool. The friction was modelled with the Karnopp friction model.

Horta, Daugherty and Martinson [7] extended the Daniels' model with active controls. Their study showed that there were high friction levels that hindered the performance of the landing gear.

One of the reasons why Amesim was chosen as the simulation tool for this thesis is the research carried out by Reineh [8]. She used Amesim to model and simulate a racing car shock absorber which yielded accurate results when compared to actual test results. As long as the original model is accurate, it is safe to assume that similar studies made with the same software will achieve accurate results.

Nevertheless, there are many effects during landing which can have a significant impact on the test results. For example, nonlinearities such as gas compression, the flow through the orifice and friction may have a significant effect on the behaviour of the shock absorber. The gas within the orifice support can be modelled as a polytropic process, but the polytropic index can have values anywhere between isothermal and adiabatic, i.e. between 1 and 1.4, as the shock absorber is never fully isolated. Furthermore, high friction levels have been observed in a combat jet shock absorber, which have been successfully modelled using the Karnopp friction model. There is much more about shock absorbers in the literature, but for the purposes of this thesis it is unnecessary to go into great detail here. As stated above, every shock absorber, especially that of a combat aircraft, is unique, so caution has to be taken when drawing general conclusions. Most of the models presented in the literature omit the effects of heat transfer, the gas mixing with the hydraulic fluid, leakage, and a variety of other phenomena, concentrating instead only on the motion of the shock absorber.

3.   THE SHOCK ABSORBER MODEL

The basis for creating a simulation model of the modified oleo-pneumatic shock absorber are its principles of operation. The model needs to accurately represent the same physical phenomena as the real shock absorber. All the main parts that affect the operation of the shock absorber have to be modelled with the same dimensions as those of a real shock absorber.

There are different methods for such modelling. Although the shock absorber could be modelled numerically, using the finite element and finite volume methods, in this thesis the modelling is done analytically. The analytical model is carried out with a commercial multi-domain system simulation software, LMS Imagine.Lab AMESim (Advanced Modeling Environment for performing Simulations of engineering systems) revision 13. This commercial software was chosen because the mathematical equations and the solver for these equations are already verified and the equations used in the model are automatically generated from a Bond graph. This saves time, which is better spent on analysing and validating the results. A Bond graph of a system is a logical decomposition of the functions of the system and shows how the different parts influence each other. The Bond graph is created from sub-models. This chapter presents the structure and the main parts of our oleo-pneumatic shock absorber, the model for the shock absorber, and the governing equations.

3.1   The main parts of the shock absorber

The modified oleo-pneumatic shock absorber can be divided into two parts according to the initial pressure: the low pressure chamber (primary chamber) and the high pressure chamber (secondary chamber). The high pressure chamber contains only nitrogen under high pressure. The low pressure chamber contains both hydraulic oil and nitrogen. The hydraulic oil and nitrogen are allowed to mix and the jet from the orifice in the upper end of the orifice support impinges on the nitrogen and may cause foaming. In the simulation model the gas and the liquid are in separate volumes, so the low pressure chamber is also divided into two parts: the primary piston assembly and the orifice support. An assembly of the modified oleo-pneumatic shock absorber, with the three parts marked, is shown in Figure 3.1. The parts are:

1) The orifice support;
2) The primary piston assembly;
3) The high pressure chamber.

The nitrogen in the two chambers cushions the impact and the hydraulic oil dampens the motion as the flow of the liquid between the primary piston assembly and the orifice support is restricted. The chambers of the modified oleo-pneumatic shock absorber are made of high strength steel, which is assumed to withstand high pressure without significant deformations. The cylinder head assembly above the orifice support is machined from a forged titanium alloy and has lugs so that the shock absorber can be installed on the main landing gear assembly. Another pair of lugs is attached to the primary piston assembly.

The shock absorber and the main landing gear form a levered suspension system. As the aircraft has the ability to land on an aircraft carrier, the stroke of the shock absorber
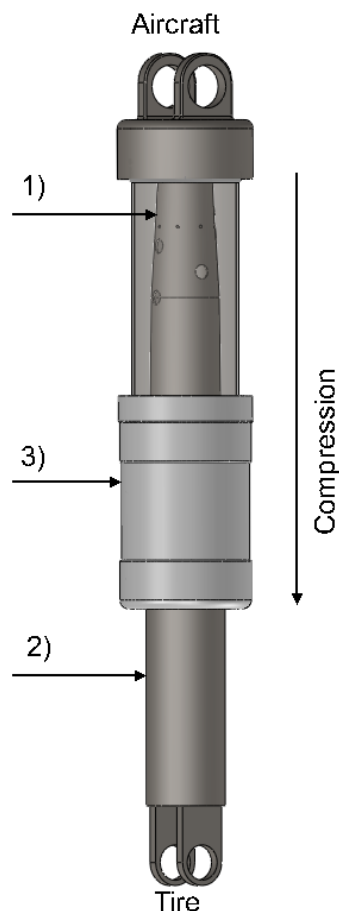

Figure 3.1. *The modified oleo-pneumatic shock absorber assembly.*
1) The orifice support, 2) the primary piston assembly and 3) the high pressure chamber.

has to be larger than that of the same aircraft that only lands on a normal runway, so a levered design has to be used as it requires less stowage space [10, p. 79].

The metering pin is attached to the end of the primary piston assembly. It has a variable shape and is responsible for the most of the damping during a stroke. At the other end of the primary piston assembly is the primary piston head. The primary piston assembly is shown in Figure 3.2., with the primary piston head and metering pin marked.

The primary piston head has small circular and square orifices, which are partially sealed by a piston ring so that the flow through the primary piston head is restricted and contributes to the damping effect of the shock absorber. The restriction caused by the piston ring varies between compression and extension, as the piston ring moves between the edges of the primary piston head. Depending on the direction of the motion, the piston ring moves between two positions, shown in Figure 3.3 with a dashed line, where 1 is the position during compression and 2 during extension. During compression the effective fluid flow area is larger than during the rebound, which means that the primary piston head has a greater damping effect during the extension than during compression.

The metering pin moves through a circular orifice on the orifice support, and it varies the flow. The orifice support has a snubber plate attached to it with shoulder bolts, which allow the snubber plate to move. There are circular holes under the snubber plate which are blocked by the snubber plate during compression and unblocked during rebound, so that the flow restriction differs depending on the direction of motion. Compared to the primary piston head, the restriction alteration is in reverse. The secondary piston head, the orifice support, snubber plate and a shoulder bolt are shown in Figure 3.4. The orifice support is enclosed by secondary piston assembly, which is not be confused with the secondary chamber, and the primary piston head moves between the faces of the orifice support and the cylinder. On the top of the second cylinder is the secondary piston head. The secondary piston head seals both the low and the high pressure chambers.
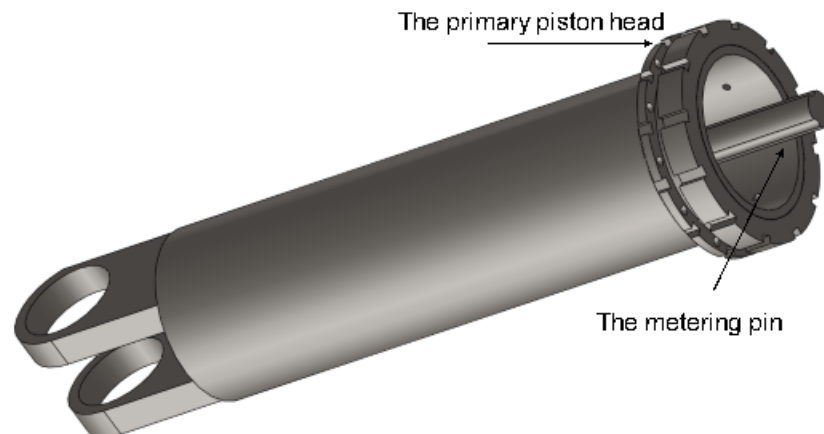
Figure 3.2. *The primary piston assembly*
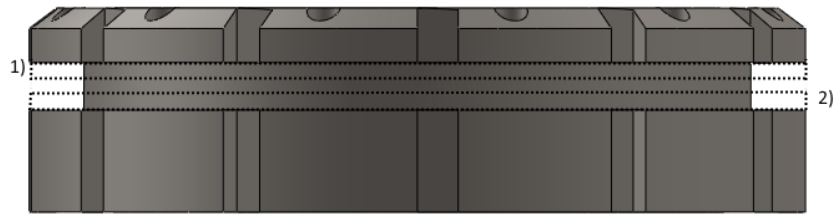
Figure 3.3. *The primary piston head and the piston ring position.1) during compression; 2) during extension.*

The high pressure chamber is a simple, gas-filled cylinder with thick walls to pre-vent deformation, as the pressure is significantly greater here than in the primary cham-ber. The secondary piston head acts as a piston head and the chamber is sealed with seals and a bushing so that the gas does not leak out of it. The primary piston assembly acts as a piston rod as it moves through the high pressure chamber during the first part of the stroke.
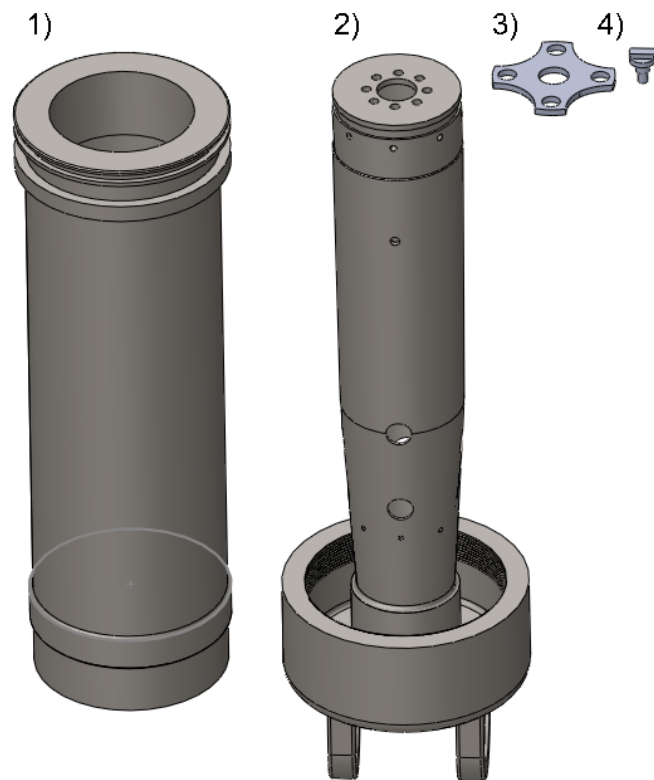
Figure 3.4. *1) The secondary piston head, 2) the orifice support, 3) the snubber plate, 4) a shoulder bolt.*

3.2   Principles of operation

The stroke of the modified shock absorber can be divided into two parts. During the initial part of the stroke, which is approximately 68 percent of the maximum stroke, only the primary piston assembly is in motion. The movement through the secondary piston assembly and the impact load is controlled by the flow of hydraulic oil through the orifice in the orifice support and by the flow through the primary piston head. The metering pin varies the cross section of the flow through the orifice in order to achieve the designed load-stroke curve. During the initial part of the stroke, the flow area through the orifice is larger than during the second part of the stroke. Near the end of the stroke, the metering pin closes the orifice, but before the metering pin is fully through the orifice the motion is forced to stop. Otherwise, the primary piston assembly would hit the orifice support, which could break the shock absorber. The pressurised nitrogen at the top of the orifice support cushions the impact load.

If the impact load is high enough, the primary piston assembly hits an end-stop, which starts the second part of the stroke, the remaining 32 percent of the maximum stroke, by forcing the high pressure side to move together with the primary piston assembly. The high pressure side is filled with highly pressurised nitrogen cushioning the high impact load, until the maximum stroke length is reached. During the rebound, the flow is less restricted, as the orifices under the snubber plate are uncovered, and the fluid is forced back to the primary piston assembly and the gas expands.

## 3.3   System model and governing equations

The schematic of the shock absorber is shown in Figure 3.5, where X_{ref} is the inertial reference position, A_L and p_L the area and the pressure of the primary piston assembly, A_{mp} the area of metering pin, p_U the pressure inside the orifice support, A_{ph} the area of the piston head, p_{ph} the pressure inside the secondary piston assembly, A_{HP} and p_{HP} the area and the pressure of the high pressure chamber, Q_1 the flow between the primary piston assembly and the orifice support, Q_2 the flow between the orifice support and the secondary cylinder, Q_3 the flow through the primary piston head and $F_{\mu 1}$, $F_{\mu 2}$, and $F_{\mu 3}$ are the friction of the primary piston assembly, viscous friction due to leakage and the friction of the high pressure chamber. The flow between the orifice support and the secondary cylinder is not restricted, as there are many large orifices between them.

The equation of motion of the shock absorber is:

$$m_{sa}\ddot{X}_{ref} = m_{sa}g - p_u A_{mp} - p_L(A_L - A_{mp}) - A_{ph}(p_u - p_{ph}) - A_{HP}p_{HP} - F_{\mu 1} - F_{\mu 2} - F_{\mu 3} \, , \qquad (1)$$

where m_{sa} is the mass of the moving parts of the shock absorber and g the gravitational acceleration. During the initial part of the stroke, the mass of the shock absorber con-
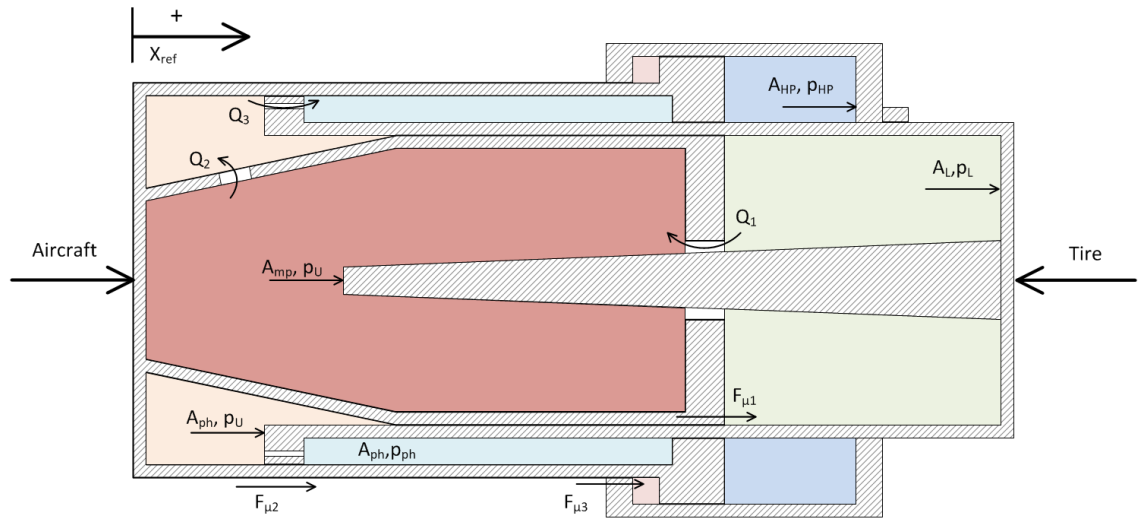
Figure 3.5. *Schematic of the oleo-pneumatic shock absorber.*

tains the mass of the primary piston assembly and the fluids within, while during the second part of the stroke, mass of the high pressure chamber is added to this.

Figure 3.6 shows a block diagram around a two dimensional cross-section of the oleo-pneumatic shock absorber. The numbered chamber submodels represent the nitrogen and hydraulic oil volumes and are shown in the cross-section. The submodels with a letter next to them represent crucial parts of the model, and a list of all the submodels used in this thesis is given in Appendix 1. The model has five chamber submodels, called either pneumatic volume or thermal-hydraulic volume. The first four form the low pressure chamber and the fifth forms the high pressure chamber. Volumes (3) and (5) are pneumatic volumes and the others are thermal-hydraulic volumes. All the chambers are rigid as the pressures are relatively low compared to the tensile modulus of the high strength steel. However, the pressure in the high pressure chamber can rise so high that the assumption of rigidity is not necessarily valid. Each one of the chambers is connected to one or more piston submodels, and together they form the main parts of the shock absorber. Volume (1) and the piston next to it represent the primary piston assembly, volumes (2) and (3), with connected pistons, form the orifice support. Volume (4), with its piston, forms the secondary piston assembly, and volume (5) and the adjacent piston represent the high pressure chamber.

The thermal-hydraulic volumes are connected to each other and there is an energy and mass balance between them. The temperature time derivative is calculated with the following equation [11, p. 45]:

$$\frac{dT}{dt} = \frac{dmh + dh + dm\left(\alpha\beta T v_s - h\right) - \alpha\beta T \dfrac{dV}{dt}}{\rho V\left(c_p - \alpha^2\beta T v_s\right)} \, , \tag{2}$$
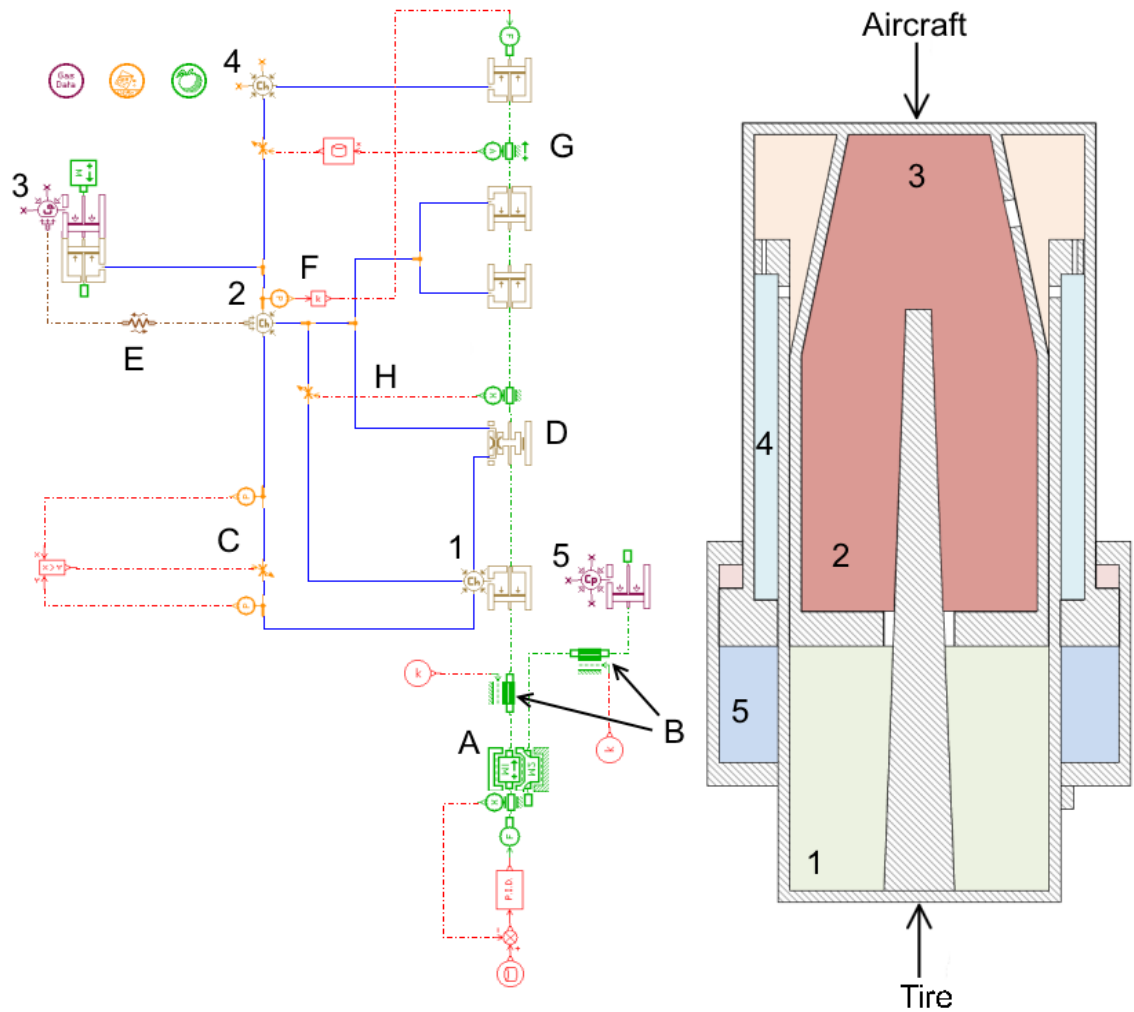
Figure 3.6. *The block diagram of the oleo-pneumatic shock absorber.*

where *dmh* is the incoming enthalpy flow rate, *dh* is the heat flow rate exchanged with the outside, *dm* is the mass flow rate through the volume, α is the volumetric expansion coefficient of the fluid, β is the bulk modulus of the fluid, *T* is the temperature of the volume, v_s is the specific volume of the fluid, *h* is the specific enthalpy of the volume, *V* is the volume, ρ is the density of the fluid and c_p is the specific heat capacity. The pressure time derivative inside a thermal-hydraulic volume is calculated from:

$$\frac{dp}{dt} = \beta \left(\frac{1}{\rho} \frac{d\rho}{dt} + \alpha \frac{dT}{dt} \right). \tag{3}$$

The temperature of the hydraulic fluid is almost constant when the shock absorber is operated, so the second part of the right hand side of Equation (3) could be neglected. However, this is not done here, as even a minor change in the fluid temperature affects the pressure inside the orifice support. The hydraulic fluid pressure inside the orifice support is determined by the gas, as the fluid and the gas are in the same volume and

therefore have the same pressure. The temperature and pressure time derivative of the pneumatic volumes (3) and (5) are evaluated by resolving the following system of two equations [12, p. 55]:

$$
\begin{bmatrix} V\left(\dfrac{\partial \rho}{\partial p}\right)_T & V\left(\dfrac{\partial \rho}{\partial T}\right)_p \\[2mm] m\left(\dfrac{\partial h}{\partial p}\right)_T & m\left(\dfrac{\partial h}{\partial T}\right)_p \end{bmatrix} \begin{bmatrix} \dfrac{dp}{dt} \\[2mm] \dfrac{dT}{dt} \end{bmatrix} = \begin{bmatrix} \sum_i \dfrac{dm_i}{dt} - \rho \dfrac{dV}{dt} \\[2mm] \sum_i \dfrac{dm_i}{dt} h_i - h \sum_i \dfrac{dm_i}{dt} + \delta Q \end{bmatrix},
\tag{4}
$$

where m is the mass of gas, dm_i/dt *(*input mass flow rate*)* multiplied by h_i *(*specific enthalpy*)* is the total enthalpy flow rate at the port i, and δQ the heat exchange with the outside. The system of equations is derived from the first law of thermodynamics, and the density and enthalpy partial derivatives depend on which equation of state is used, discussed further in Subsection 3.2. From this system of equations, the pressure inside the orifice support, p_U in Equation (1), can be calculated. As can be seen in Figure 3.6, volumes (2) and (3) are connected with a generic conduction model (E). This simulates the heat exchange between the gas and oil, as they are in the same volume in reality.

The mass envelope (A) incorporates the masses of both the low (inner mass) and high pressure chambers (envelope), the viscous friction of the system and the stroke length and end-stops. The mass envelope is connected to the input signal submodel of the system and the PID-controller below the mass envelope allows the model to receive different forms of input signals, such as force or displacement signals. The symbol of the mass envelope is shown in Figure 3.7. for the sake of clarity.

When the two masses in the submodel come into contact, there is a contact force. The contact force is calculated depending on whether the contact is at its lower or higher limit. When the shock absorber is fully extended, the contact force for the lower limit is used, and when the initial stroke is completed and the inner mass hits the envelope, the higher limit contact force is used. The contact force appears when the relative position between the inner mass and the envelope exceeds the maximum displacement. The magnitude of the force is related to the difference between the relative and max-
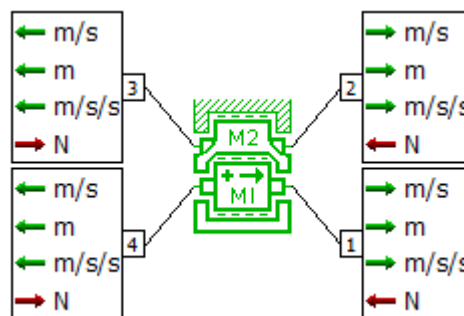

Figure 3.7. *The symbol of the mass envelope [13].*

imum displacement, thus it is related to time, and causes fluctuation in the velocity and acceleration of the inner mass and the envelope. The lower limit contact force is [13]:

$$F_{min} = \begin{cases} Kb_{min}(X_{min} - X_{rel}) - Db_{min}\left(1 - e^{\frac{-(X_{min} - X_{rel})}{Pd_{min}}}\right)V_{rel} & \text{if } X_{rel} < X_{min} \\ 0 & \text{if } X_{rel} \geq X_{min} \text{ ,} \end{cases} \tag{5}$$

and the higher limit contact force is:

$$F_{max} = \begin{cases} Kb_{max}(X_{rel} - X_{max}) + Db_{max}\left(1 - e^{\frac{-(X_{rel} - X_{max})}{Pd_{max}}}\right)V_{rel} & \text{if } X_{rel} > X_{max} \\ 0 & \text{if } X_{rel} \leq X_{max} \text{ ,} \end{cases} \tag{6}$$

where $Kb_{min/max}$ is the lower/higher limit stiffness, $X_{min/max}$ the lower/higher displacement limit, X_{rel} is the relative displacement of the two masses, $Db_{min/max}$ is the lower/higher limit contact damping coefficient, $Pd_{min/max}$ is the lower/higher limit penetration for the full damping and V_{rel} is the relative velocity. The force on the inner mass is then calculated from [13]:

$$\begin{aligned} F_{\text{sum}1} = F_{ext4} - F_{ext1} + F_{min} - F_{max} + F_{min3} - F_{max3} + g\, m_1 \sin(\theta) \\ - R_{visc1} V_{rel} - W_1 V_{rel}^2 sign(V_{rel}) \text{ ,} \end{aligned} \tag{7}$$

where F_{ext1} is the force acting on port 1, F_{ext4} is the force acting on port 4, $F_{min3/max3}$ is the contact force between the inner mass and a fixed reference calculated from Equations (5) and (6), g is the gravitational acceleration, m_1 is the mass of the inner mass, θ is the angle of inclination, R_{visc1} is the viscous friction between the piston and the envelope and W_1 is the windage friction between the piston and the envelope. If the relative position between the inner mass and either the envelope or the fixed reference are between the minimum and maximum displacement, all the F_{min} and F_{max} terms disappear from the equation. Furthermore, windage is not taken into account, as the air resistance is considered insignificant. The force on the envelope is calculated from [13]:

$$\begin{aligned} F_{\text{sum}2} = F_{ext3} - F_{ext2} - F_{min} + F_{max} + F_{min2} - F_{max2} + g\, m_2 \sin(\theta) \\ + R_{visc1} V_{rel} + W_1 V_{rel}^2 sign(V_{rel}) - R_{visc2} V_2 + W_2 V_2^2 sign(V_2) \text{ ,} \end{aligned} \tag{8}$$

where F_{ext3} is the force acting on port 3, F_{ext2} is the force acting on port 2, $F_{min2/max2}$ is the contact force between envelope and the fixed reference calculated from Equations (5) and (6), m_2 is the mass of the envelope, V_2 is the velocity of the envelope and W_2 is the

windage friction between the envelope and the fixed reference. Now the acceleration of the inner mass can be calculated from [13]:

$$a_1 = \frac{dV_1}{dt} = \frac{d^2 X_1}{dt^2} = \frac{F_{sum1} - F_{dry}}{m_1} \, ,$$

(9)

and for the envelope:

$$a_2 = \frac{dV_2}{dt} = \frac{d^2 X_2}{dt^2} = \frac{F_{sum2} + F_{dry}}{m_2} \, ,$$

(10)

where F_{dry} is the dry friction force or static and Coulomb friction. As the friction is modelled by two friction submodels F_{dry} is nil for both the inner mass and the envelope.

There are two friction submodels (B) above the mass envelope. These are needed to correctly model the friction, because the coefficients of friction differ between the low and the high pressure chambers. One friction model is connected to the primary piston assembly, and it models $F_{\mu1}$, and the other friction model is connected to the high pressure chamber, and it models $F_{\mu3}$, in Equation (1). Friction force is calculated using the Karnopp model with the Stribeck effect [14, pp. 84-85]:

$$\begin{aligned} F_{fric} &= min\left(|F_E|, F_S\right) sign\left(F_E\right) \quad \text{and} \quad v = 0 \qquad \text{if} \, |v| < dv \\ F_{fric} &= \left(F_C + \left(F_S - F_C\right) e^{-3|v|/v_s}\right) sign(v) + F_V v \quad \text{if} \, |v| > dv \, , \end{aligned}$$

(11)

where F_E is the external force applied on the body, F_S is the stiction force, F_C is the Coulomb friction force, v is the relative velocity, v_S is the Stribeck velocity, dv is the zero velocity interval and F_v is the coefficient of the viscous friction. The values for the static, Coulomb and viscous frictions were determined by a series of batch runs, from which the values that most closely agreed with measured tests, were chosen.

An estimation of the normal force between a piston ring and a cylinder can be calculated from [2, p. 265]:

$$F_N = \frac{1}{2} A_s (\Delta p) \, ,$$

(12)

where A_s is the outer surface area of the seal and Δp is the pressure difference between the two sides of the piston. The piston friction force can then be calculated from:

$$F_{FP} = \mu_C F_N = A_{PF} \Delta p \, ,$$

(13)

where μ_C is the Coulomb friction coefficient and A_{PF} is the effective piston ring area:

$$A_{PF}=\frac{1}{2}\pi\mu_C D_p L \ , \tag{14}$$

where D_p is the external diameter of the piston and L is the seal ring axial length. According to equations (12 to 14), varying the initial pressure inside the shock absorber affects the friction levels, so depending on the initial pressure inside the shock absorber, fricion forces are set according to:

$$F_{C/S}=F_{C/S,ns}\frac{p_{init}}{p_{ns}} \ , \tag{15}$$

where $F_{C/S,ns}$ is the Coulomb or static friction force used during normally serviced shock absorber simulation, p_{init} is the initial pressure and p_{ns} is the normal service pressure.

The behaviour of the friction force is shown in Figure 3.8, where V is velocity and F is force. Without the Stribeck effect, when the velocity differs from zero the friction force instantly changes from static friction to Coulomb friction and then, as the velocity increases, the viscous friction also increases. The Stribeck effect allows a transition between the friction terms that follows an exponential function, so the discontinuity between stiction and Coulomb friction disappears. In the simulation, this is manifested as a decrease in the stick-slip phenomenon and is the main advantage of the Karnopp friction model with the Stribeck effect. According to [15, p. 1716], the Karnopp model with the Stribeck effect is efficient to solve, but the zero velocity interval does not match the actual friction. However, the Karnopp model is widely used and is accurate enough for the simulation purposes.
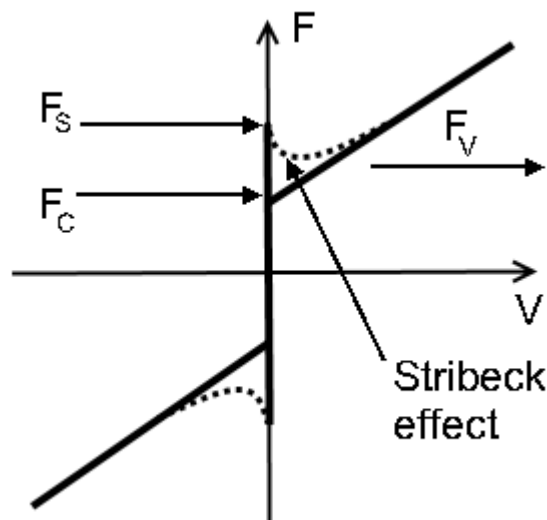

Figure 3.8. Friction forces and the Stribeck effect.

It is assumed that there is leakage of hydraulic oil between the primary piston assembly, the orifice support and the second piston assembly. Leakage has a negative effect on the damping ability of the shock absorber, but it is difficult to limit it. It is simulated using a submodel for leakage with viscous friction (D) that computes the hydraulic leakage past a piston. The values for the parameters of the submodel are selected so that a single submodel can be used to govern all the leakage. As the exact amount of leakage is unknown the values are selected carefully, and on the whole it is assumed that any leakage only has a minor effect on the shock absorber operation. The leakage submodel simulates the laminar leakage between a cylindrical piston and a cylindrical sleeve, with the corresponding viscous friction force. The volumetric flow rate through the leakage is calculated from [13]:

$$Q = \frac{r_c \pi d_p}{2}\left(v^+ + v^- - \frac{\Delta p\, r_c^2}{6\mu l_c}\right),$$

(16)

where r_c is the radial clearance, d_p is the external piston diameter, v^+ and v^- are the velocities of the envelope and the piston, Δp is the pressure difference between ports, μ is the dynamic viscosity of the fluid and l_c is the contact length. The friction force on the piston is:

$$F^- = -\Delta p\, \pi \frac{d_p - d_c}{2} r_c + \mu l_c\left(v^+ - v^-\right)\pi \frac{d_p - d_c}{r_c},$$

(17)

where d_c is the clearance between the envelope and the piston. The friction force on the envelope is:

$$F^+ = -\Delta p\, \pi \cdot \frac{d_p - d_c}{2} r_c - \mu l_c\left(v^+ - v^-\right)\pi \frac{d_p}{r_c}.$$

(18)

The viscous friction, $F_{\mu 2}$ in Equation (1), is:

$$F_{\mu 2} = F^-$$

(19)

and the enthalpy flow rate at the upstream side of the leakage is:

$$dmh_{up} = dm_{up} h\left(p_{up}, T_{up}\right),$$

(20)

where h is the enthalpy of the liquid at upstream pressure and temperature. Then, by applying the conservation of energy, the downstream enthalpy rate is obtained:

$$dmh_{down} = -dmh_{up} - F^+ v^+ - F^- v^- \, . \tag{21}$$

There are three variable thermal-hydraulic restrictions in the model: the snubber plate (C), the metering pin (H), and the primary piston head (G). The snubber plate is between pressure sensors which are connected to a submodel that makes a comparison between the inputs, so if the pressure in the primary piston assembly is greater than the pressure in the orifice support, the snubber plate is pressed down on top of the orifice support and the circular orifices are closed. If the pressure in the primary piston assembly is lower than the pressure in the orifice support, the orifices are open and fluid flows through them to the primary piston assembly.

The cross section of the metering pin varies with the stroke. In the model, the metering pin restriction submodel has a displacement sensor connected to it. The submodel receives displacement information from the sensor and uses an ASCII table to choose the corresponding value for the cross section. The metering pin is responsible for most of the damping, and therefore the accuracy of the metering pin submodel is important for the overall performance of the model. The normalised cross section of the metering pin against normalised displacement is shown in Figure 3.9. There are three different constant values that are taken from the drawings of the metering pin, and the change between them is instantaneous. After these, the cross section is defined by two piecewise linear functions that reach zero value, when the stroke is at the maximum. In fact, a real metering pin varies more in shape than the modelled version, but modelling its exact shape would require precise measurements of the dimensions of the metering pin, and this was simply not feasible here.
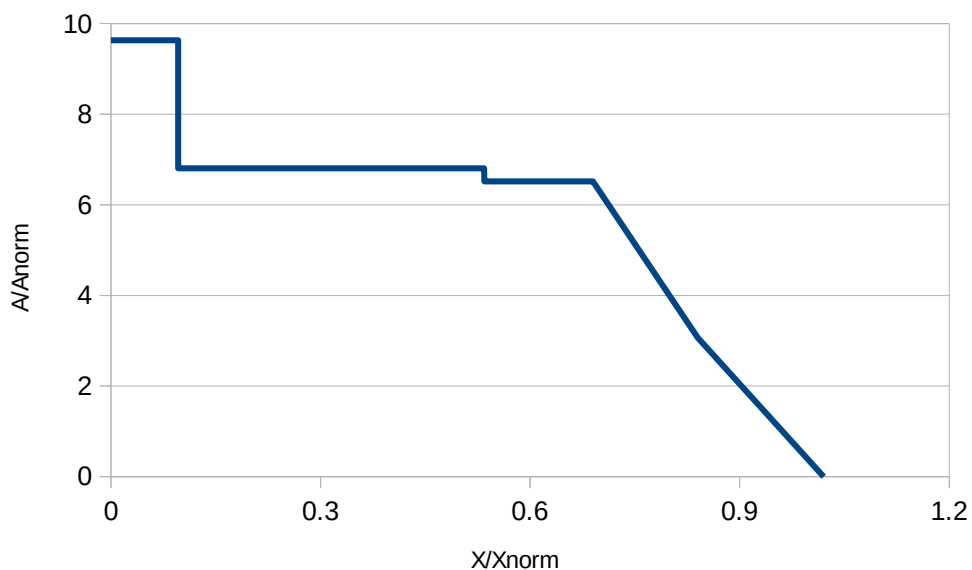

Figure 3.9. *The normalised cross section of the metering pin against normalised displacement.*

The restriction submodel of the primary piston head is similar to the metering pin restriction. It is also controlled by an ASCII file, but it has a velocity sensor connected to it instead of a displacement sensor, as the position of the piston ring depends on the direction of the motion, rather than the position of the primary piston head. The mass flow rate through a variable thermal-hydraulic restriction is calculated from [13]:

$$dm = c_q A \sqrt{(2 \rho \Delta p)} , \qquad (22)$$

where c_q is the flow coefficient and A is the cross section of the orifice. The flow coefficient is defined as:

$$c_q = c_{qmax} \tanh\left(\frac{2\lambda}{\lambda_{crit}}\right) , \qquad (23)$$

where c_{qmax} is the maximum flow coefficient, λ_{crit} is the critical flow number and λ is the flow number, which is calculated from:

$$\lambda = \frac{D_h}{\nu} \sqrt{\left(\frac{2|\Delta p|}{\rho}\right)} , \qquad (24)$$

where ν is the fluid kinematic viscosity and D_h is the hydraulic diameter. The flow number needs to have a variable flow coefficient, otherwise dm against ΔP has an infinite gradient in Equation (22), which is not realistic [13]. The restriction submodel is an adiabatic component, which means that all the energy dissipated in the restriction is transferred to the liquid and the outlet temperature is calculated from:

$$T_{out} = T_{in} + v(1 - \alpha T_{in})\frac{|\Delta p|}{C_p} , \qquad (25)$$

where v is the specific volume, α is the volumetric expansion coefficient of the fluid, and C_p is the specific heat of the fluid. The pressure inside the primary piston assembly, p_L in Equation (1), and the pressure inside the secondary piston, p_{ph}, can be calculated from the Equation (22).

Modelling the primary piston head and the metering pin as restrictions produces an error as it doesn't account for the forces acting on the metering pin and the primary piston head, so these forces must be added to the model. This is done by adding a submodel that converts signal input into force (F). The submodel is connected to a pressure sensor and the pressure signal is then multiplied by the missing annulus areas of the primary piston head and the metering pin to obtain the acting force, which is calculated from:

$$F = p_U \left(A_{ph} + A_{mp} \right), \tag{26}$$

where F is the missing force that needs to be added, A_{ph} is the annulus area of the primary piston head and A_{mp} is the annulus area of the metering pin. Both of these terms are shown in Figure 3.5. and are present in Equation (1). The piston submodels have two ports and the force at the positive port, shown with arrows in the submodel symbol, is calculated from:

$$F_1 = F_2 + \frac{\pi}{4} \left(P_P - P_{atm} \right) \left(dp^2 - dr^2 \right), \tag{27}$$

where F_2 is the force at the negative port of the piston, P_P is the pressure inside the piston, P_{atm} is atmospheric pressure, dp is the piston diameter and dr is the diameter of the piston rod. As the model is built with a series of pistons, the force at the positive port of a certain piston is the force at the negative port of another piston, depending on the direction of the submodel. When all the forces are added together, along with the friction forces calculated with Equation (11), and the missing forces calculated with Equation (26), the variables in Equation (1) are defined.

3.4   Modelling the gas

The gas inside the orifice support and the high pressure chamber is nitrogen. This can be modelled as either a perfect gas, an ideal or a semi-perfect gas, or as a real gas. Modelled as perfect gas, it follows the established ideal gas law and has constant specific heat capacities. The semi-perfect gas model also follows the ideal gas law, but the specific heat capacities follow polynomial functions. The ideal gas law is only accurate at low pressures and temperatures [16, p. 136] as the volume of the gas particles are ignored. However, inside an aircraft main landing gear shock absorber the pressure can rise so high that the ideal gas law is no longer valid, so a real gas model has to be used for this thesis.

   Amesim offers four different equations of state for real gas calculations: van der Walls, Redlich-Kwong, Redlich-Kwong-Soave and Peng-Robinson. The equation of van der Walls is one of the earliest attempts to predict real gas behaviour and, according to [20, p. 289], does not agree well with experimental results, and therefore it should not be used. The Redlich-Kwong-Soave equation is a modified version of the Redlich-Kwong equation and is, according to [17], more accurate [18]. The Peng-Robinson equation, on the other hand, not only behaves similarly to the Redlich-Kwong-Soave equation, but also predicts the liquid density values better [19], so the Peng-Robinson equation of state is used in the simulation cases presented in this thesis. The Peng-Robinson equation of state is:

$$\left(P+\frac{a\,\alpha(T)}{v_s^2+2\,bv_s-b^2}\right)(v_s-b)-rT=0 \,, \tag{28}$$

where P is the pressure, T the temperature, r is the specific gas constant and v the specific volume, which is defined as:

$$v_s=\frac{V}{m} \,, \tag{29}$$

where V is the volume and m is the mass of the gas. The attractive term a is calculated from:

$$a=0.45724\frac{r^2 T_c^2}{P_c} \,, \tag{30}$$

where T_c is the critical temperature and P_c the critical pressure. The covolume b is calculated from:

$$b=0.0778\frac{r\,T_c}{P_c} \tag{31}$$

and the alpha-function is,

$$\alpha(T)=\left[1+m\left(1-\sqrt{\frac{T}{T_c}}\right)\right]^2 \,, \tag{32}$$

where m is:

$$m(\omega)=0.37464+1.54226\,\omega-0.26992\,\omega^2 \tag{33}$$

and ω is the Pitzer's acentric factor:

$$\omega=-1-\log_{10}\left(\frac{P_{sat}}{P_c}\right)_{T=0.7T_c}. \tag{34}$$

The compressibility factor of a real gas is defined as:

$$Z=\frac{P}{\rho\,r\,T} \,, \tag{35}$$

where ρ is density. For a perfect or semi-perfect gas the compressibility factor is equal to 1 and for real gas calculations it is deduced from the equation of state used. Other gas properties, such as absolute viscosity, constant pressure specific heat and thermal conductivity follow second order polynomial functions with different empirical coefficients for each gas.

3.5 Modelling the hydraulic fluid

The hydraulic fluid used in the shock absorber is based on synthetic hydrocarbon and satisfies the requirements of the Mil-H-83282 specification. The fluid has a wide operating temperature range, from -40°C to +205°C, and has good oxidation and thermal stability. The additives added to the fluid provide corrosion resistance, anti-wear and anti-foaming protection.

As with the gas modelling, the thermal-hydraulic properties of the hydraulic oil follow high order polynomial functions. Specific volume, absolute viscosity, specific heat constant pressure and thermal conductivity are defined by these functions and are used to define the isothermal bulk modulus, the volumetric expansion coefficient, the kinematic viscosity and the thermal diffusivity, thus defining the thermal liquid fully.

Isothermal bulk modulus is calculated from:

$$\beta = \frac{-v_s}{\left(\dfrac{\partial v_s}{\partial p} \right)_T} \ , \tag{36}$$

where v_s is the specific volume taken from the polynomial expression. The volumetric expansion coefficient of the oil is:

$$\alpha_V = \frac{1}{v_s} \left(\frac{\partial v_s}{\partial T} \right)_P \ . \tag{37}$$

The kinematic viscosity of the oil is:

$$\nu = \frac{\mu}{\rho} \ , \tag{38}$$

where μ is the dynamic viscosity of the oil and the thermal diffusivity of the oil is:

$$\alpha_T = \frac{k}{\rho c_P} \ , \tag{39}$$

where k is the thermal conductivity of the hydraulic oil.

3.6   Solving the differential equations

It is not within the scope of this thesis to discuss the methods of integrating differential equations, but the integration algorithms used by Amesim are presented here, as they are based on well-known integration methods. The system of equations generated from the Bond graph of the modified shock absorber model consists of ordinary differential equations defining state variables of the system. There are two widely used methods for integrating ordinary differential equations: the well-known explicit Runge-Kutta methods and linear multistep methods [21, pp. 5-6]. Amesim uses the latter, which is a modified version of LSODA [22]. This scheme changes the linear multistep method used between Adams code, a high order Adams-Moulton method [23, p. 111] and Gear's method [24]. The Adams code is well suited for ordinary differential equations for non-stiff problems, and the integration starts with this method. LSODA analyses the characteristics of the equations, and if stiffness is detected, the integration method is switched to Gear's method, which is an algorithm for stiff problems.

4.   MODEL VALIDATION

According to [25, p. 293], validation is the process of determining how accurately a model represents the real world. This is done by comparing measured test results to simulation results. The modified oleo-pneumatic shock absorber has measured data available from a static test bench, a dynamic test system and a real landing. Depending on the test system used, different attributes are measured. The most important attributes of the oleo-pneumatic shock absorber during compression are pressure, displacement and velocity. The stiffness, friction and damping effect of the shock absorber can be analysed with these attributes. An exact match between experimental and simulation data is rare, as errors and uncertainty are part of modelling and simulation. However, if the model behaves correctly during each test case, and the results are accurate enough, when compared to a designated level, the model can be considered valid. Furthermore, the model is built to perform well overall. A minor tweak to the parameters can be made without compromising the model, which could improve the performance of the model in one type of simulation case, but decrease it in another. In this chapter, the static test measurements are compared to the simulation model and then to the dynamic test and a real landing.

4.1   The static case

The test system for the static case has a hydraulic cylinder, which is controlled by a PID-controller. The hydraulic cylinder is attached to the end of the shock absorber and the other end of the shock absorber is rigidly braced to prevent it from moving. The hydraulic cylinder is used to induce the compression and thus the extension of the shock absorber. During the test, a pressure sensor in the hydraulic piston measures the pressure, and a displacement sensor measures the displacement of the hydraulic piston rod. The force acting on the shock absorber is calculated from the pressure. The PID-controller controls the stroke of the hydraulic cylinder so that the shock absorber is compressed to the same degree during each individual test.

The test is, in fact, quasi-static, because the load applied on the shock absorber is progressively increased. However, the compression occurs so slowly, the velocity being less than 0.03 m/s, that the damping effect is not apparent in the results. The displacement measured in the static case test is given as an input signal to the simulation model, and the measured force is then compared to the simulated force; the normalised input

signal is shown in Figure 4.1. The stroke used is approximately 88 percent of the maximum stroke, which is regarded as typical stroke measured during a real landing.

Figure 4.2. shows a normalised force-displacement curve of an unpressurised shock absorber, where the blue curve is the measured result and the red curve is the simulation result. Initially, the measured force has a peak in the force-displacement curve. It then decreases and settles at a certain level, until the initial stroke is complete, and the high pressure side engages. As long as there is no change in the Coulomb friction, the force measured on the high pressure side should also be constant because the velocity is constant. However, the force increases during the latter part of the stroke. The high pressure side has a charge valve with a small diameter. While the shock absorber is unpressurised, there is air inside, which is forced through the charge valve during unpressurised compression. This could well explain the force increment during the latter part of the stroke.

The initial peak is due to the static friction, and when the shock absorber starts to move there is a transition to Coulomb friction. The model also predicts a peak at the beginning, but the transition from static friction to Coulomb friction is faster. At the end of the initial stroke, before the high pressure side engages, the curve has a decreasing slope, indicating a decrease in friction. This decrease can be explained by the improving lubrication between the contacts. The simulation model behaves similarly when the friction force is changed during compression. However, the change in the friction force is very small compared to the forces measured during the normal service pressure test, and therefore friction can be kept constant during the simulation, without any noticeable errors. Both curves show oscillation around the constant friction force, which is due to the stick-slip effect, as the external force compressing the shock absorber is just enough to
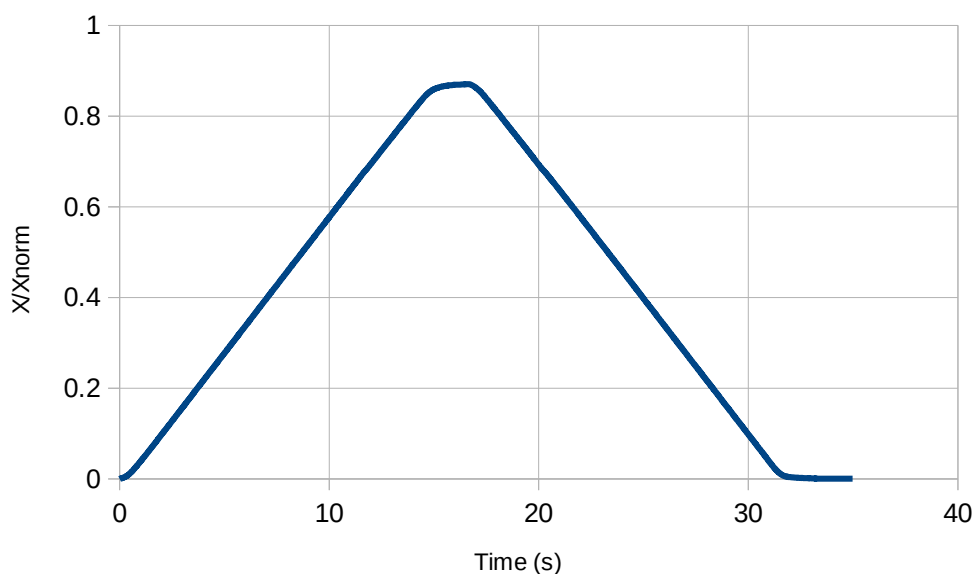

Figure 4.1. *The normalised displacement used as an input signal in the static case simulation.*
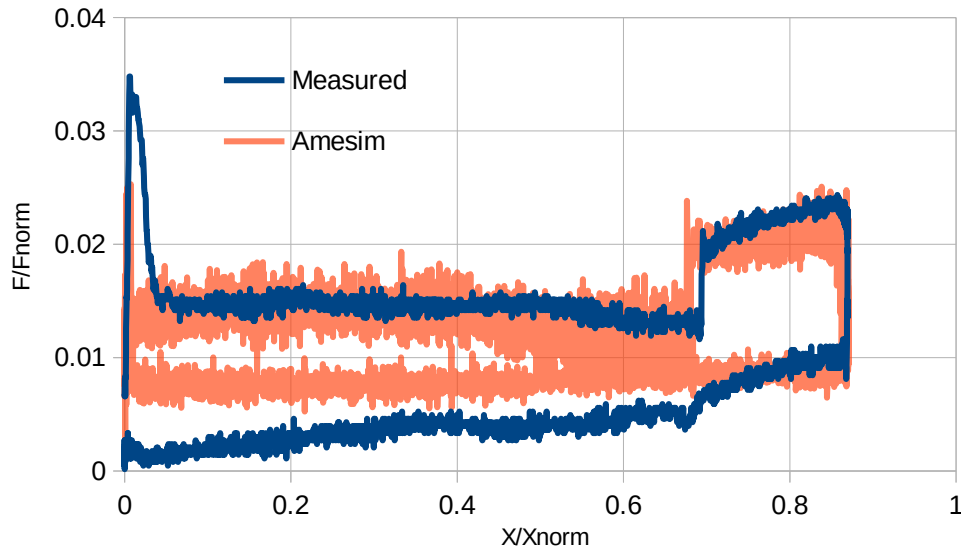
Figure 4.2. *A normalised force-displacement curve of an unpressurised modified shock absorber.*

make the shock absorber move, changing the friction level from static friction to Coulomb friction.

When the shock absorber is pressurised, the friction force increases due to the greater pressure difference on the sides of the seals and bearings. The initial friction levels were first defined by the unpressurised case, and then the final values were defined using batch runs of different friction values, by changing the Coulomb and static friction forces in Equation (11), and using the normally serviced shock absorber case.

The importance of a correct friction value can be seen in the normalised force-displacement curve of a shock absorber with normal service pressure, which is shown in Figure 4.3, where the blue curve is the measured result, the red curve is the simulation result with friction and the dashed-line green curve is the simulation result without either friction or heat transfer between the gas and the liquid. The two simulation results reveal a significant difference of approximately 13 percent in the force that is required to engage the high pressure side. The high friction level needs further examination, although, according to [7, p. 15], a static friction force close to 9 kN was measured during an A6-intruder shock absorber study, so high friction levels are not unknown in aircraft shock absorbers.

When the initial pressure is lowered, so are the friction levels which are calculated from Equation (15). A normalised force-displacement curve of a shock absorber with a quarter service pressure is shown in Figure 4.4. The simulation, also done with quarter friction levels, produces accurate results. This indicates that the friction level used in the normally serviced shock absorber simulation is correct and the friction levels should be set according to the pressure inside the shock absorber, as suggested in [2, p. 265].
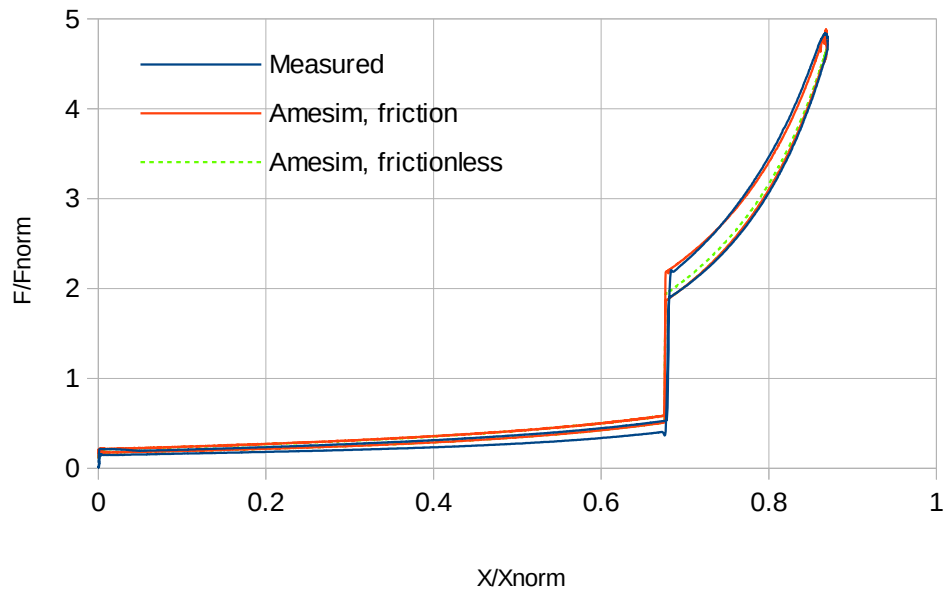
Figure 4.3. *A normalised force-displacement curve of a normally serviced shock absorber.*

Friction is the prime reason for the hysteresis in the curves, as it always opposes the movement. The friction force has positive or negative values depending on whether the shock absorber is compressed or extended, and this leads to the hysteresis. Another contributory factor is so-called thermal hysteresis [26, p. 11], which is work lost as heat between compression and expansion. The model presented in this thesis does not change energy with its surroundings, but the generic conduction model (E) does transfer heat from the gas to the liquid, so the heat transfer has an effect on the hysteresis on the
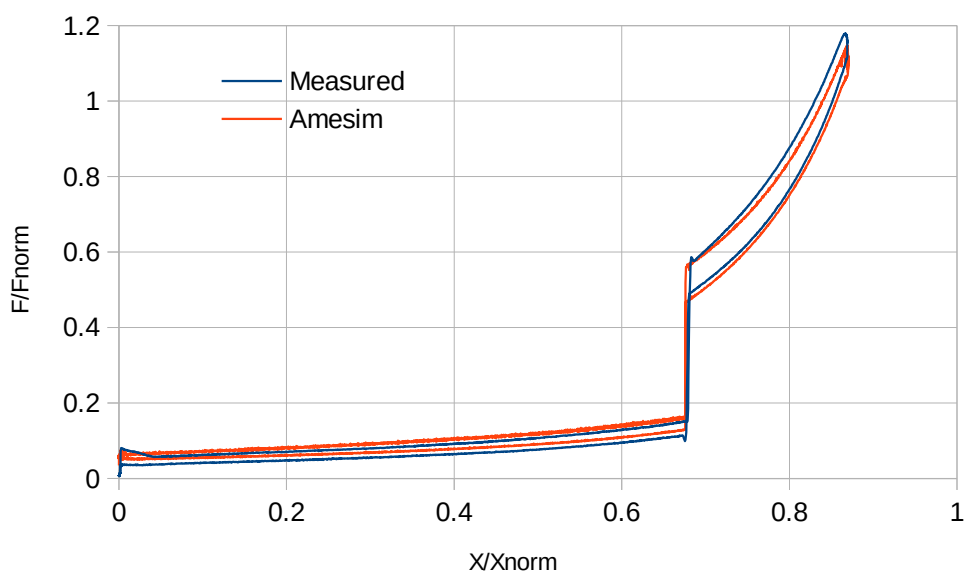

Figure 4.4. *A normalised force-displacement curve of a shock absorber serviced with quarter pressure.*

low pressure side. The exact amount of heat transferred between the gas and liquid is difficult to define, as the heat transfer depends on the mixing of the two phases. It is reasonable to assume that the convective heat transfer is much greater during a real landing than during static compression. This indicates that more detailed analyses and measurements are needed to fully understand the heat flow. Furthermore, during a real landing the velocity of the aircraft can be so high that the heat loss from the surface of the shock absorber into its environment might be significant.

The vertical line between the hystereses in the results of both normal and quarter service pressure simulations is in the right place and roughly the same size as the measured ones. During the initial stroke, the model seems to be stiffer than the real shock absorber. The exact quantity of nitrogen in the shock absorber is unknown, but it can be calculated from the original drawings, where the quantity of hydraulic oil is specified. Even a small error in the estimation of the quantity of gas has a significant impact on the results, and this explains the difference in stiffness.

4.2 The dynamic case

The dynamic test is performed with a nitrogen actuator, which has a tank of highly pressurised nitrogen. The nitrogen operates a cylinder, attached to the end of the shock absorber, whose other end is rigidly braced. The shock absorber can thus be compressed rapidly, simulating the first impact of a real landing. It is difficult to conduct dynamic tests with the shock absorbers of an aircraft main landing gear because the forces and the rate of changes are so great that the requirements for a hydraulic pump becomes impractical, so there is no hydraulic test system. It is also difficult to make the test system immune to disturbances, as the high force levels produce intense vibration so the measured signal has a lot of noise which can be hard to distinguish from the original signal.

The normalised force used as an input signal is shown in Figure 4.5. The force was measured during a dynamic test, and the velocity and the displacement of the shock absorber was compared to the measured results from the same test. After the steep slope at the beginning of the input signal, the force settles down to a virtually constant value.
The velocity curve should exhibit similar behaviour. There should be a peak at the beginning, and when the force settles to a constant the velocity should incline to zero. The dynamic case is also used to find the correct parameters for the viscous friction in Equation (11) with batch runs.
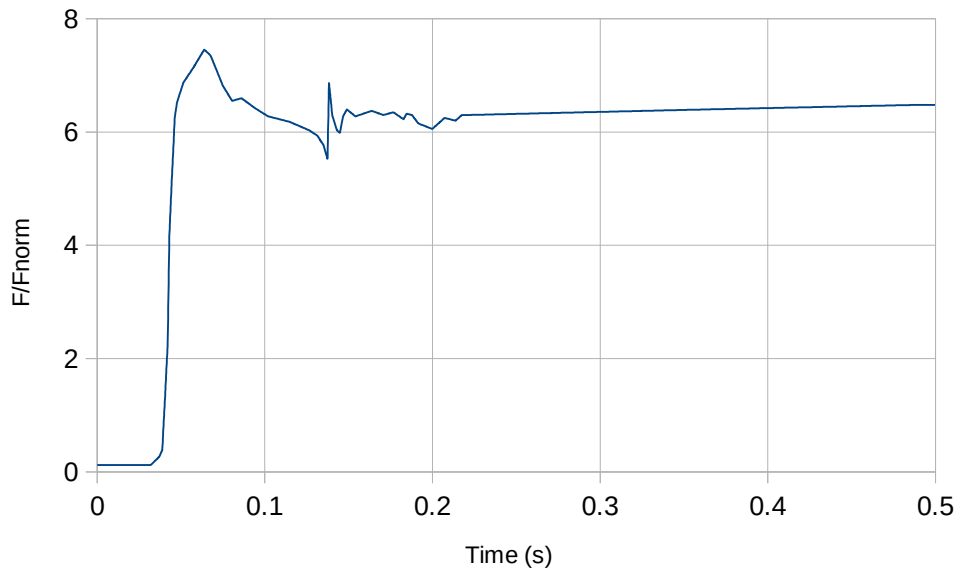
Figure 4.5. *The normalised force used as an input signal in the dynamic case simulation.*

During the dynamic test, the normalised velocity of the modified shock absorber measured from the top of the primary piston assembly is shown in Figure 4.6. The simulation closely matches the measured curve during the initial peak and at the end. However, after the first part of the stroke, when the high pressure side engages, there is some fluctuation. The reason for the fluctuation is the end-stops, and the parameters defining their behaviour, and these are incorporated in the mass envelope submodel used in the model. The fluctuation can be reduced by changing the values of the higher limit penetration for full damping and the higher limit contact damping coefficient, in Equations
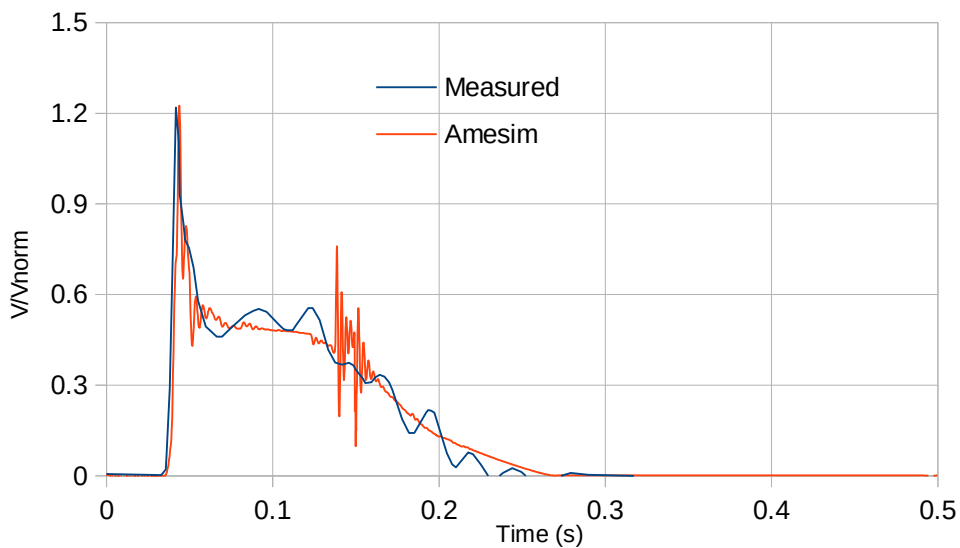

Figure 4.6. *The compression velocity during the dynamic test.*

(5) and (6), when calculating the high contact force. However, this impinges on the overall performance of the model. Because the accuracy of the measurements is unknown, it is possible that the fluctuation is not recorded during the test. The mass envelope submodel could be replaced with a mass system with ideally plastic end-stops, which would resolve the problem, but there is no doubt that more information about the measurements is needed.

The model reaches zero velocity approximately 0.05 seconds later than the real shock absorber. This indicates that the damping force of the model is higher than in reality. The less the fluid flow is restricted, the faster the primary piston assembly completes the initial stroke, at which point the velocity reaches zero. This is confirmed by the normalised displacement results, which are shown in Figure 4.7. The maximum displacement is the same for both the model and a real shock absorber, but the real shock absorber reaches the point of maximum displacement faster.

This is due to the inaccuracy of the metering pin submodel, as explained in Chapter 3.1, and also a possible error in the volume of the nitrogen in the orifice support. Nevertheless, overall the model produces results that closely match the actual measured results.
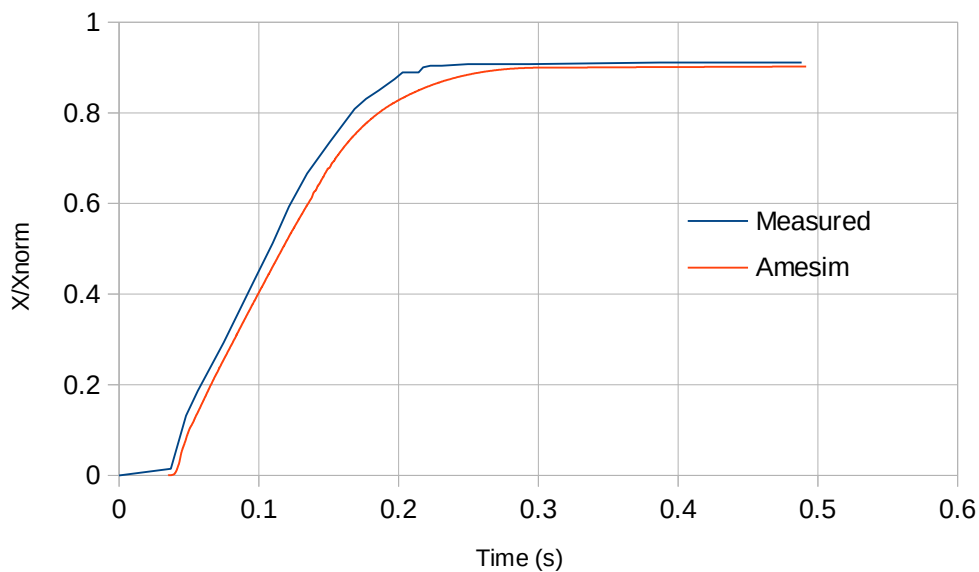

Figure 4.7. The displacement during the dynamic test.

4.3 Real landing

The final validation is done by analysing the pressure inside the shock absorber. The pressures from the orifice support and the high pressure chamber have been measured during a real landing. These pressures are compared to the pressure simulated by the model. The most important part of this comparison is the initial contact with the ground, 'touchdown'. During touchdown the shock absorber undergoes the greatest external

load that occurs during a landing, which is manifested as a high initial peak in the pressure and displacement. Therefore, this is the most likely moment for a malfunction in the shock absorber. After the peak, the shock absorber has a series of gradually diminishing shorter strokes due to the damping effect of the shock absorber, which continue until a state of equilibrium is reached.

The displacement measured during the landing is used as an input signal during the simulation. The normalised displacement of the shock absorber is shown in Figure 4.8. The stroke recorded during the landing is close to the stroke used in the static case measurements, and as expected, the highest peak is measured during touchdown. After the two initial peaks, the displacement is close to a constant value. The reason for this is that the load is not large enough for the high pressure side to engage, but the initial stroke of the low pressure side, or the first 68 percent of the maximum stroke, is completed.

The normalised pressure inside the orifice support is shown in Figure 4.9, where the blue curve is the measured pressure and the red is the simulated pressure. The simulated pressure accurately follows the measured pressure during the initial peak. However, after the first two peaks the simulated pressure diverges from the measured pressure.

There is an unknown quantity of leakage from the shock absorber to its surroundings during landing, and this has an effect on the pressure inside the shock absorber. This leakage has not been modelled here, as it would require a plethora of calculations and measurement which are beyond the scope of this thesis. Furthermore, the amount of nitrogen in the orifice support also affects the pressure level during landing.
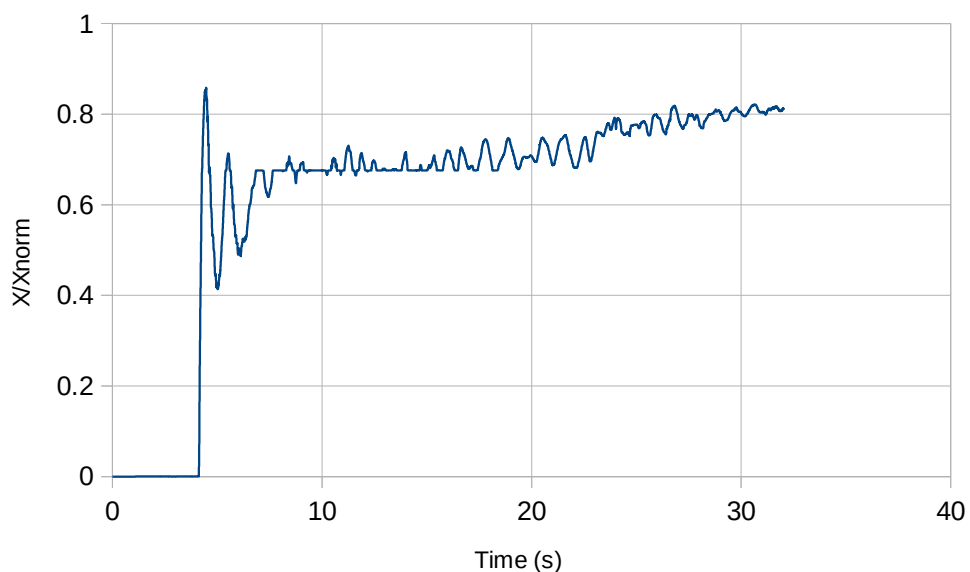

Figure 4.8. *The normalised displacement of the shock absorber measured during landing.*
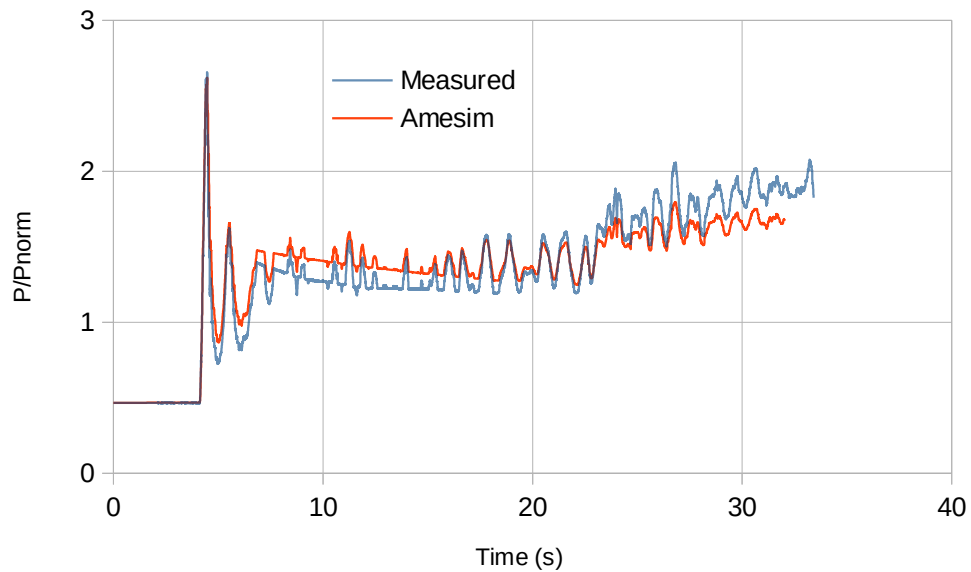
Figure 4.9. *Normalised pressure inside the orifice support during landing.*

Figure 4.10 shows the normalised pressure within the high pressure chamber. The simulated pressure closely matches the measured pressure. Although the model predicts all the peaks in the pressure almost perfectly, the model does have too high values during the last ten seconds of the landing. As stated earlier, the shock absorber model does not account for energy exchange with the surroundings. The temperature of the nitrogen within the high pressure chamber rises rapidly, warming the solid parts of the shock absorber. This is manifested as a difference in the ambient temperature and the surface of the shock absorber, leading to heat exchange, which lowers the pressure within the high pressure chamber. This heat exchange can be neglected during the dynamic and static test cases, but should be considered in longer simulations, such as the landing simulation, whose duration is tens of seconds. The aircraft's landing velocity, and ambient wind velocity contribute to the convective heat transfer during landing, which makes the heat transfer case sensitive. Nevertheless, the model predicts the initial peak in pressure in both the orifice support and the high pressure chamber regardless of any heat exchange with the surroundings.
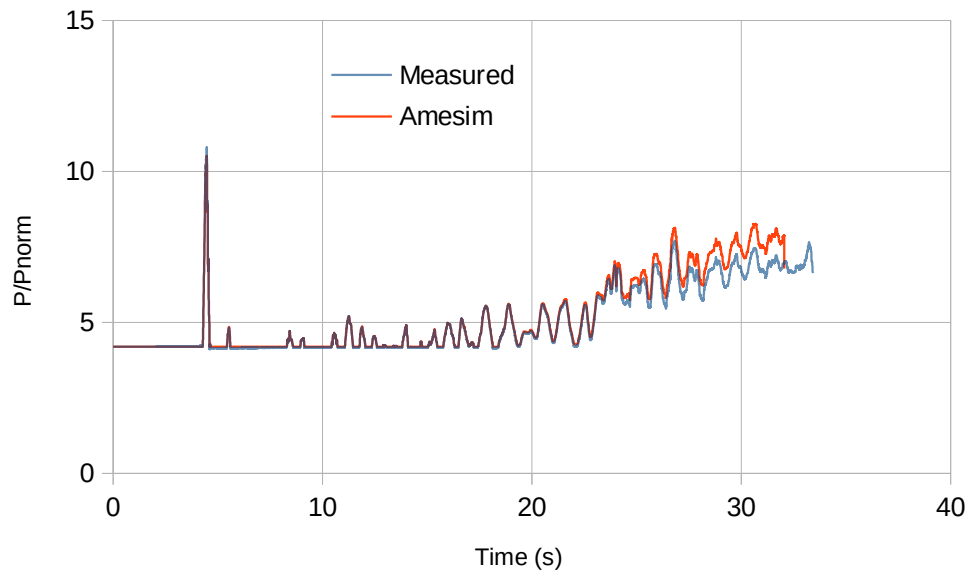
Figure 4.10. *Normalised pressure inside the high pressure chamber during landing.*

5. UTILIZING THE SIMULATION FOR CONDITION MONITORING AND FAULT DETECTION

One of the objectives of this thesis is to investigate the possibilities of utilizing the simulation model as a tool in condition monitoring and fault detection. Combat jets are used in extreme conditions and there can be situations when normal maintenance procedures are impractical or infeasible, such as when the combat jets operate from a temporary airfield, or during any crisis when maintenance time might be limited. Changing a main landing gear shock absorber takes a long time, during which the combat jet is out of operation. Therefore, it is important to develop condition monitoring and fault detection methods that minimise the downtime due to maintenance.

Usually, the shock absorber is inspected before every take-off. A pressure gauge attached to the low pressure chamber is used to check the pressure, and if the pressure is below the normal service pressure, nitrogen is added to the shock absorber. If there is considerable leakage during landing and multiple consecutive landings are made, the ratio between the nitrogen and the hydraulic liquid might become distorted, thus increasing the risk of malfunction. Pressure gauges are often inaccurate and have a tendency to break down, so a new instrument which can measure both pressure and temperature is clearly needed. The ideal measuring device would also have the ability to tell whether, the shock absorber needs to be serviced and refilled with hydraulic fluid by measuring the pressure and temperature values during landing. This measuring device would compare the characteristics of the pressure behaviour, i.e. the amplitudes and frequencies of the pressure fluctuations during landing. It would compare those values to the predefined values produced by simulation and real-life measurements, and if the values differ the device should indicate that the shock absorber needs to be serviced.

This chapter first discusses the results from simulations varying the gas-liquid ratio in the model by changing the amount of nitrogen. Then, simulations with different initial temperatures, and those in which the shock absorber is heated or cooled, are discussed, along with the implications for the service procedure. This chapter concludes with a broader discussion of the proposed new measuring device, and the factors contributing to the predicted values.

5.1 The effect of variations in the gas-liquid ratio on the operation of the shock absorber

As stated above, there is a change so that the ratio between the nitrogen and the hydraulic liquid in the lower piston assembly becomes distorted after a while. An unknown quantity of gas and liquid leaks from the shock absorber into the environment during each landing. The current practice is that if a quick check reveals that the pressure inside the shock absorber is low, nitrogen is added. This affects the operation of the shock absorber, as the more nitrogen there is in the low pressure chamber, the less the pressure rises when the shock absorber is compressed.

One major limitation in the model presented here is that it is built so that its hydraulic fluid volumes (1, 2 and 3 in Figure 3.6) have the physical dimensions of the shock absorber incorporated into them. The volume of the hydraulic fluid in the shock absorber can be controlled simply by changing these dimensions. However, this would mean that the actual dimensions of the shock absorber would change, which is not realistic. If the diameters of the pistons next to the volumes are changed, this directly affects the forces acting in the system, cf. Equation (27). The only other option would be to change the length of the pistons, which would mean that the maximum stroke would change. Furthermore, if the hydraulic volumes were to be replaced by the pneumatic volumes the model would have to be validated again. Therefore, only the nitrogen volume (4 in Figure 3.6) is changed. This is achieved by changing the length of the adjacent piston when the gas-liquid ratio is varied. As this induces a certain error on the simulation results, only a qualitative analysis can be made. This limitation, and a proposed solution for it, are discussed in Chapter 7.

The volume of the nitrogen within the orifice support ranges from 100 percent, which is the normal volume of a serviced shock absorber, to 160 percent at 20 percent intervals. Figure 5.1. shows the force-displacement curve of the static case simulations with the different nitrogen volumes. The larger the volume of the nitrogen, the lower the force needed to compress the shock absorber, because the pressure increases more slowly. On the low pressure side, the nonlinear behaviour of the gas spring disappears, as the amount of nitrogen within the shock absorber is increased. In the 160% case, the force-displacement curve is almost a constant on the low pressure side, and there is little resistance during compression. The vertical line, which is the difference between the maximum force of the low pressure side and the force needed to engage the high pressure side, stays constant, as the high pressure side is not varied in the simulation. As the length of the vertical line is constant and the forces on the low pressure side are smaller, the high pressure side engages with less force and the maximum force decreases as nitrogen is added to the system. As the presented model is limited, no comprehensive analysis of the dynamic case can be made. If the hydraulic liquid is replaced with nitrogen,
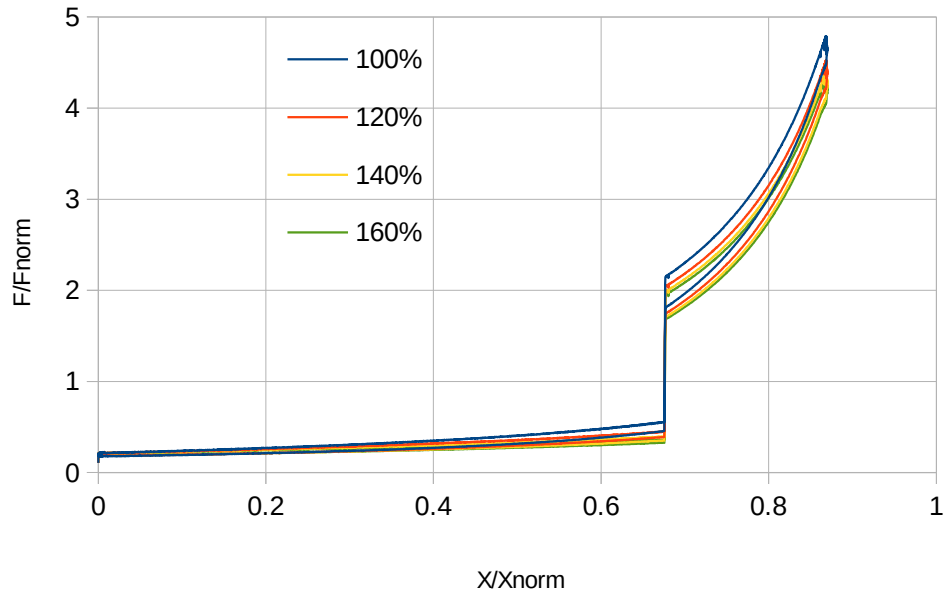
Figure 5.1. *Force-displacement curves of the static case simulation with varying nitrogen volume.*

the damping effect of the shock absorber decreases. This should appear as faster compression velocities in the dynamic case simulations. When only nitrogen is added, the velocity difference between the simulations is very low and therefore is not shown.

Figure 5.2 shows the displacements during the dynamic case simulation with varied nitrogen volumes. Adding nitrogen affects the stiffness of the shock absorber so that when more nitrogen is added, the maximum displacement increases. However, different simulation cases reached the maximum displacement at approximately the same time,
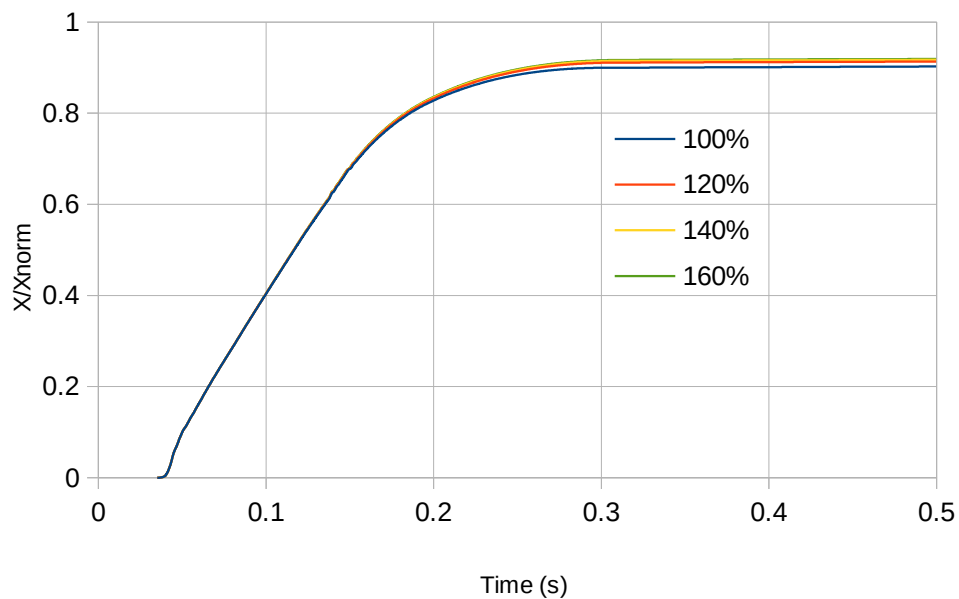

Figure 5.2. *Displacement during the dynamic case simulation with varying nitrogen volume.*

exposing one of the limitations of the model. It is important that the model is improved in the near future so that it can incorporate all the relevant physical phenomena.

Varying the nitrogen volume affects the pressure levels during compression. This can be seen in Figure 5.3, where the initial nitrogen volume is varied for the simulated landings. There are significant differences between the normally serviced shock absorber and the one with 20 percent more nitrogen, so even a relatively small change in the nitrogen volume can have considerable effect on the operation of the shock absorber. If the right side of the Equation (4) is kept constant and the volume on the left side is increased, the rate of pressure and temperature must decrease, which is manifested as lower pressure inside the orifice support.
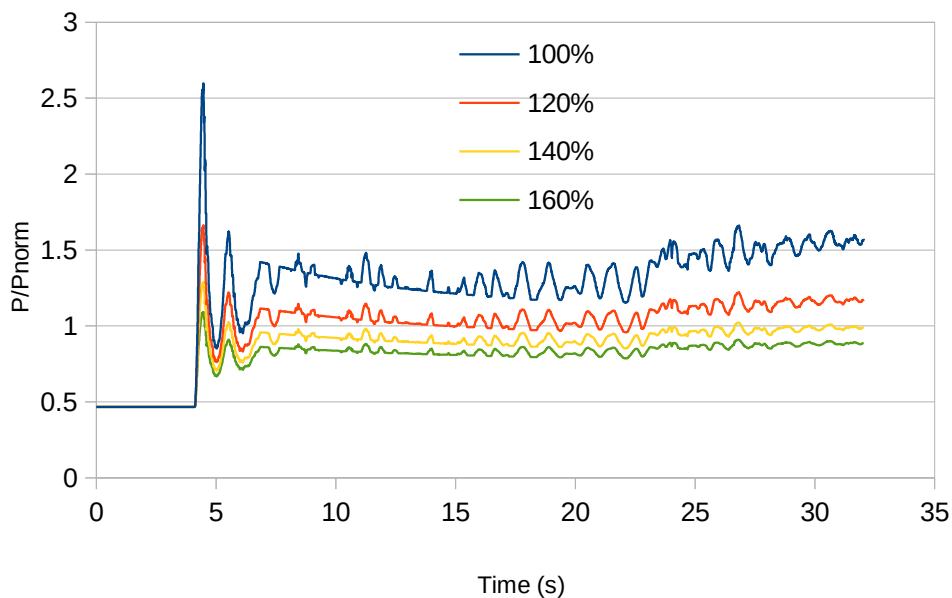

Figure 5.3. Simulated normalised pressure inside the orifice support during landing with varying nitrogen volume.

5.2 The effect of temperature variation on the pressure behaviour

The temperature within the shock absorber is dependent on the atmospheric temperature. The shock absorber temperature may differ from the atmospheric temperature when the shock absorber is inside the fuselage of the aircraft, but the landing gear must be extended before landing can take place so any temperature difference quickly disappears. The shock absorber's operating temperature can vary greatly, as the aircraft is used in different countries with widely different climates.

Figure 5.4 shows the effect of varying initial temperature on the pressure behaviour inside the orifice support during landing. The simulation is done with two different initial temperatures representing the upper and lower extremes of +40 °C and -40 °C.
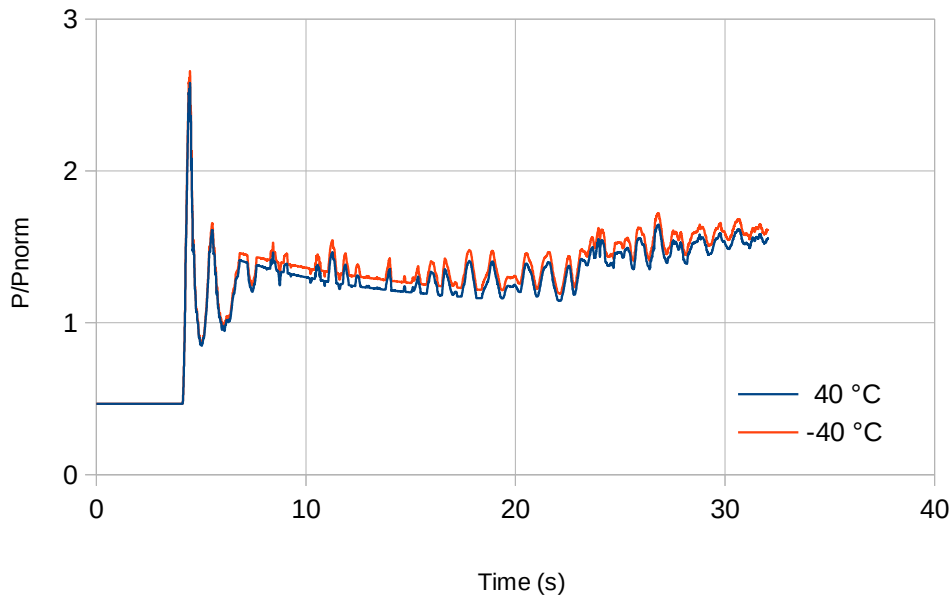
Figure 5.4. *Simulated normalised pressure inside the orifice support during landing with varying initial temperature.*

These extreme values have been selected, because most operating temperatures on Earth are between these two values and the difference between the results can be seen clearly. Amesim calculates the initial mass of the nitrogen in the orifice support using the initial temperature as a reference temperature for the density. Hence, a simulation with a different initial temperature actually simulates a case where the shock absorber is filled with fluid and gas that have been stored at that initial temperature. During the simulations, the lower the initial temperature, the greater the rise in the pressure. Because, nitrogen is denser when it is cold, the shock absorber can be filled with more nitrogen in terms of mass, which offsets the effect of the lower temperature on the pressure behaviour. In fact, the difference between the two extreme cases is small, and it can be assumed that the initial temperature of the fluid during servicing has little impact on the pressure behaviour of the shock absorber.

Next, the model is modified so that the nitrogen is heated to +40 °C or cooled to -40 °C from the same initial temperature, which was +20 °C. This simulates a case where the shock absorber has been filled inside a heated maintenance building, and then exposed to the atmospheric temperature before landing. The pressure behaviour inside the orifice support during landing, when the nitrogen is heated up or cooled down, is shown in Figure 5.5. Depending on whether the shock absorber is heated or cooled, the pressure increases or decreases accordingly after exposure to the atmospheric temperature.

In these simulations, the results differ from each other significantly. In both cases, the initial pressure inside the orifice support is the service pressure. After that, the shock absorber is either heated or cooled depending on the case. During this stage, the pres-

sure rises or drops, and this change in pressure is significant, especially in the case with cooling. The greatest difference between the two cases occurs at the initial peak. As might be expected, the lower the atmospheric temperature, the lower the initial peak.

The heating and cooling of the shock absorber also affects the overall displacement. Warmer hydraulic fluid has lower viscosity than cooler fluid, and therefore the viscous friction due to leakage is also smaller, which can easily be deduced by analysing equations (17) and (19). This means that with the same shock, the overall displacement is greater when the shock absorber is warmer. The displacements when the shock absorber is heated to +40 °C and cooled to -40 °C, are shown in Figure 5.6.

Normally, when the shock absorber is serviced and the fluids are changed, the service is done indoors in a warm maintenance building. The quantity of hydraulic fluid is based on volume, i.e. the shock absorber is filled with a certain volume of fluid as defined in the service manual. Once the service volume in the shock absorber has been reached, the flow of hydraulic fluid is stopped and the shock absorber is then filled with nitrogen until a specified pressure is reached. This means that the nitrogen mass can vary depending on the indoor conditions. It also means that there may be a considerable difference between the indoor and outdoor temperatures, which may have an effect on the operation of the shock absorber.

This makes servicing the shock absorber based on pressure problematic. As shown, the pressure inside the orifice support may differ significantly from the service pressure, if there is a large temperature difference between the servicing conditions and the outdoor conditions, or if the service conditions change, which also affects the pressure behaviour. This indicates that the shock absorber should always be serviced in the outdoor conditions in order to ensure the optimal operation of the shock absorber. The problem
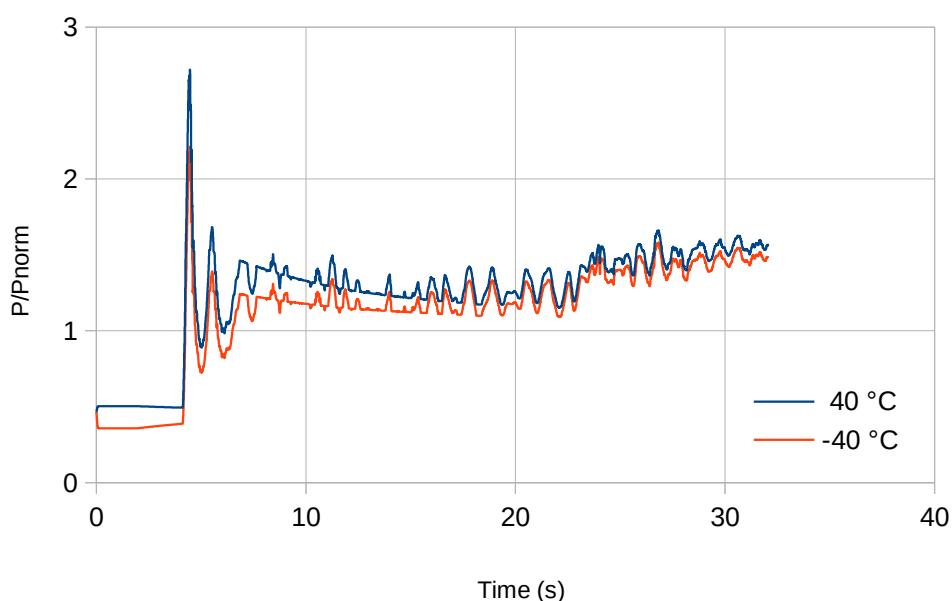

Figure 5.5. *Simulated normalised pressure inside the orifice support during landing, when the shock absorber is heated to 40 °C and cooled to -40 °C.*

with this is that when the shock absorber is removed from the landing gear, the aircraft has to rest on a support structure. This makes outdoor servicing extremely difficult, which is why servicing is normally done indoors. These factors also affect the new measuring instrument as temperature variation has a great impact on the pressure behaviour and its characteristics.
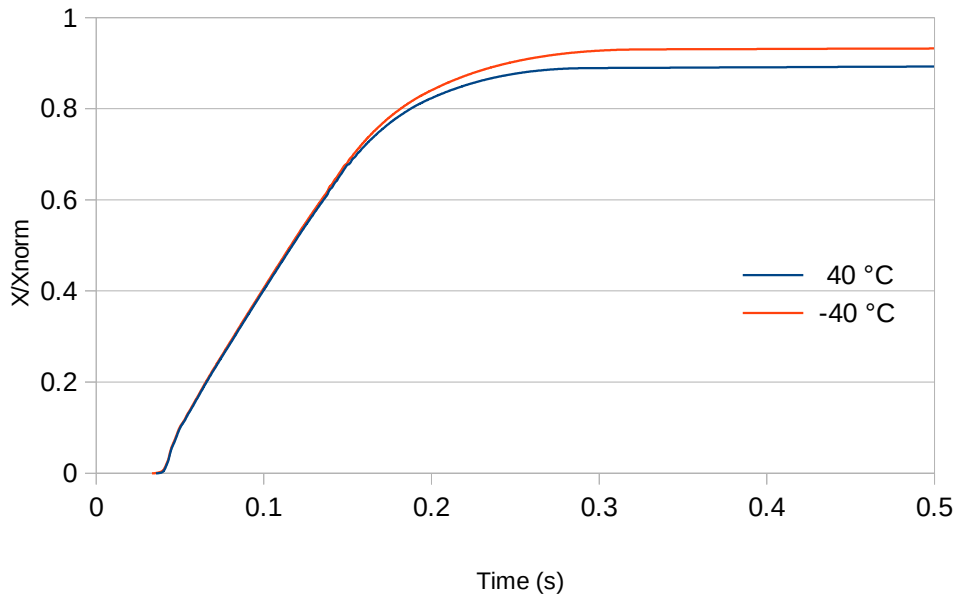

Figure 5.6. Displacement during dynamic case simulation, when the shock absorber is heated to 40 °C and cooled to -40 °C.

Overall, temperature has a significant role on the pressure behaviour inside the shock absorber, but the significance of these variations on the operation of the shock absorber, and thus on the main landing gear is difficult to analyse without modelling the whole landing gear assembly. With regard to the main landing gear, the most important part of a shock is the first moment, when all the links in the main landing gear are supposed to lock. This happens during the first few millimetres of the stroke. If the locking fails, the landing gear assembly allows the wheel to move sideways, which causes the aircraft to become uncontrollable on the ground, something which is highly undesirable during a real landing. Although varying the gas-liquid ratio or the temperature does not appear to affect the first part of the stroke in an adverse way, a more detailed analysis has to be conducted with an improved model in order to be sure of this.

5.3   Discussion on the new measuring instrument

The new measuring instrument has the ability to measure the pressure and the temperature inside the orifice support. The objective is that the new instrument can tell when the pressure behaviour differs from the expected normal pressure behaviour. Depending on

the degree of difference, the instrument should indicate whether the shock absorber needs to be serviced soon, or whether it should be serviced immediately.

With current practice, it is difficult for a maintenance crew member to read the pressure from the small pressure gauge on the shock absorber. The new measuring device would be connected to a series of indicator lights (green, yellow and red), which would be easy for the maintenance crew to see from afar. A green light would indicate that the shock absorber is operating properly, yellow that the shock absorber should be serviced soon and red that servicing is required immediately. These states should be ascertained by analysing the amplitudes and frequencies of the pressure fluctuations which occur during landing. This is only a preliminary discussion, as the project of developing the new measuring instrument has only just begun and the design and the exact properties of the instrument are still under discussion.

The pressure behaviour inside the orifice support is temperature-dependent. At a certain temperature inside the orifice support, a corresponding pressure behaviour can be expected. The effect of temperature variation on the operation of the shock absorber is discussed in more detail below, in Subsection 5.2. The pressure behaviour is also dependent on the initial pressure, the weight of the aircraft, and the landing itself as the angle of the aircraft and its sink speed also affect the pressure behaviour and the gas-liquid ratio, as explained above. Although the initial pressure should be set according to the service manual, the service pressure has a range of 0.7 bar in the lower pressure chamber and 1.4 bar in the high pressure chamber and this has a slight effect on the expected pressure behaviour. The effects of the initial conditions will have to be taken into consideration as the new measuring instrument is designed and developed.

The weight of the aircraft varies according to the mass of the fuel in the aircraft's fuel tank and the armaments it is carrying. The weight can vary significantly, as the maximum take-off weight is twice the aircraft's weight, although the aircraft is not designed to land at its maximum take-off weight. Increased weight means increased sink speeds and higher impact loads can be expected. In addition, depending on the roll, pitch and yaw of the aircraft during landing, the impact load might not be distributed evenly between the two main landing gear shock absorbers.

All of the above variables will have to be taken into consideration when the new measuring instrument is being designed. The model presented in this thesis is limited to one-dimensional motion, so the effects of roll, pitch and yaw are not simulated. The weight of the aircraft and the damping and cushioning effects of the tires can be added to the model, but the best solution would be to incorporate the model into a larger model made with other software, which can simulate the varying roll, pitch and yaw and the motion of the aircraft and has the landing gear modelled.

The values for the normal pressure behaviour, which depend on the initial values of the factors discussed in this chapter, can be defined with the help of simulations combined with real-life measurements. However, finding the limits of the normal and abnor-

mal pressure behaviour is a difficult task, because so many variables have an effect on the shock. There is also a high risk that an imperfect landing would make the new measuring instrument indicate that service is needed, even though the shock absorber has been operating correctly. Be that as it may, a series of measurements has to be carried out during the design phase so that the measuring instrument can be verified and validated.

6.   MODEL LIMITATIONS AND FUTURE IMPROVEMENTS

The accuracy of the simulation model defines the accuracy of its results. The model presented in this thesis is still under development, and there are still some properties missing. Although the current model produces results close to reality, it has some limitations and exhibits some non-realistic behaviours. This chapter discusses the limitations and non-realistic behaviour of the model and proposes some solutions to these problems.

6.1   Gas-liquid interaction

One major flaw in the model presented in this thesis is the separate modelling of the nitrogen and the hydraulic oil on the low pressure side. This limits the use of the model to cases where the volume of the hydraulic fluid is constant. This is because the volume is directly linked to the physical dimensions of the shock absorber, so changing one would inevitably mean changing the other. In the near future, the model will be used to simulate cases in which the shock absorber is underfilled, but the model must be improved before this can be done.

In the orifice support of a real oleo-pneumatic shock absorber, the nitrogen and the hydraulic liquid are in the same volume and some of the nitrogen is absorbed into the liquid. This affects the properties of the liquid in that the greater the quantity of dissolved nitrogen, the greater the change in the fluid's properties. The quantity of the dissolved gas depends on the particular gas and liquid used and the temperature and the partial pressure of the gas. This quantity can be considerable if there is chemical affinity between the two phases [2, p. 177]. Even two essentially immiscible liquids can form an emulsion, which, of course, has different properties than a pure liquid. If the volume of the gas significantly exceeds that of the liquid, the emulsion may become a foam [2, pp. 179-180].

Because the compressibility of a perfect gas is the reciprocal of the gas pressure and usually larger, even at high pressures, than that of a liquid, even a small mass fraction of gas can have a dramatic effect on the compressibility of the liquid [2, p.184]. On the other hand, calculating the exact amount of dissolved gas is a complex process as there are so many factors contributing to it, and the underlying physics is still not fully understood [27, p. 4]. It is also worth noting that an oleo-pneumatic shock absorber should be designed so that nitrogen and hydraulic oil are not in the same volume and should be

separated [10, p. 81]. Another point is that the jet of hydraulic fluid that issues from the orifice should be deflected so that it does not impinge on the nitrogen, as this may generate froth and affect the compression process by cooling the nitrogen [28, p. 187].

The gas content is defined as:

$$x = \frac{V_{gas}(P_{atm}, T_0)}{V_{liq}(P_{atm}, T_0) + V_{gas}(P_{atm}, T_0)} \, , \tag{40}$$

where V_{gas} is the volume of the dissolved gas and V_{liq} is the volume of liquid under the reference conditions. The reference conditions are atmospheric pressure, $P_{atm,}$ and a temperature of 273 K, T_0. The gas content follows the linear Henry's law [2, p. 177]:

$$p = K_H x \, , \tag{41}$$

where p is the partial pressure of the gas and K_H is the Henry's law constant.

Equation (41) is modified so that all the gas becomes undissolved before zero pressure. When the partial pressure is at the saturation pressure or above, all of the gas is dissolved, and when the partial pressure is low enough, all the gas is undissolved. Henry's law is valid between these two points, and there is some free gas and some dissolved. This is shown in Figure 6.1, where P_{sat} is the high saturation pressure and P^H_{vap} is the low saturation pressure. When the high saturation pressure is reached, all the gas that was initially free has been dissolved into the liquid. When the pressure is lower than $P^H_{vap,}$ some vapor is formed due to cavitation, but all the gas is free. If the pressure decreases even further, a certain pressure level is reached at which all the liquid is vaporized so that only vapour and free gas exist. The density and the dynamic viscosity of the
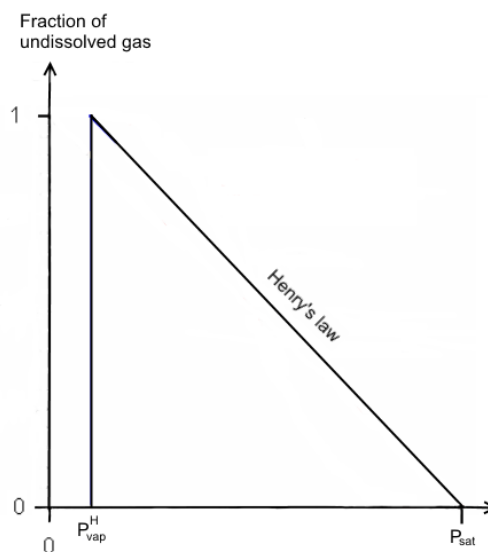

Figure 6.1. *Modified Henry's Law*

liquid are calculated from equations that depend on the pressure of the liquid. These equations are beyond the scope of this thesis, but more information can be found in [27].

Modelling the gas-liquid interaction is done by changing the pneumatic volume, Volume (3) in Figure 3.6, to a thermal-hydraulic volume, as shown in Figure 6.2. This enables the cavitation/aeration calculations in the Amesim fluid data submodel, which incorporates the parameters for the gas content, calculated with Equation (40), the high and low saturation pressures, the effective molecular mass of the vapour, the absolute viscosity of the gas, and the polytropic index. The values for the effective molecular mass of the vapour and for the absolute viscosity are those of nitrogen. The polytropic index is not a constant in real-life situations, but according to [6, p. 14] an average value is usually sufficient. This can be selected by analysing the dynamic behaviour of the shock absorber.

The pressure of the free gas within the thermal-hydraulic volumes when cavitation/aeration is enabled follows the polytropic process [27, p. 7]:

$$p = K \cdot \rho^{\Gamma} , \tag{42}$$

where K is a constant, ρ is the density of the fluid and Γ is the polytropic index. The bulk modulus is calculated from:

$$B = \Gamma \cdot p . \tag{43}$$

From these equations, it is easy to see that the value of the polytropic index has a considerable effect on the solution of a simulation, as the bulk modulus is directly proportional to it. The lower and higher saturation pressures also have to be calculated carefully, as they define the domain of validity for the modified Henry's law.

The temperatures and pressure behaviours in the orifice support during the static case simulation, with cavitation/aeration either disabled or enabled are shown in Figure 6.3.
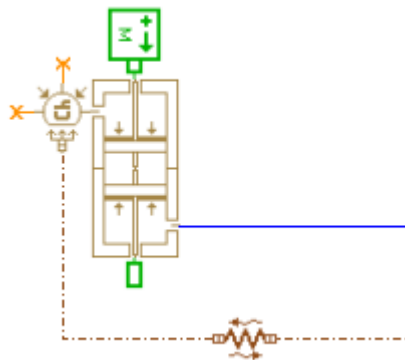

Figure 6.2. *Changes done to the model, when gas-liquid interaction is considered.*
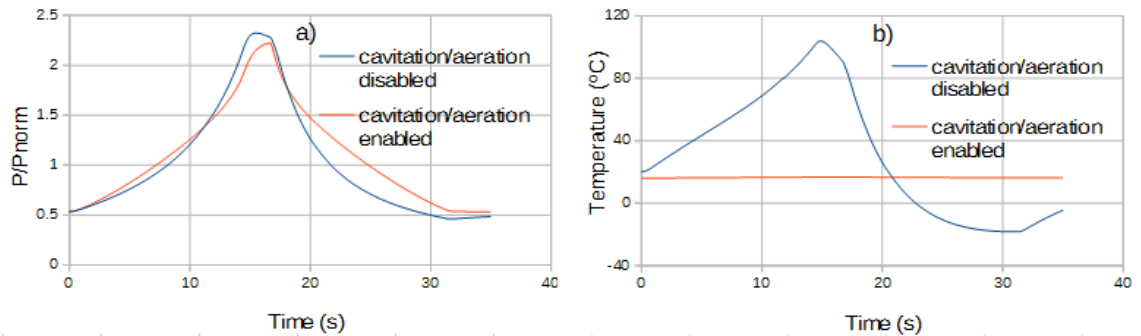
Figure 6.3. *Static case simulation with cavitation/aeration enabled and disabled.*
a) The pressure; b) The temperature inside the orifice support.

The case with the cavitation/aeration enabled has not yet been validated, as there is some uncertainty about some of the values of the variables discussed in this chapter. Therefore the results could not be used in this thesis. However, the results are still shown to faciliate discussion of the differences between the two models.

The simulations with the cavitation/aeration enabled, were done using 1.4 as the value for the polytropic index, which makes the process adiabatic. The pressure rises and decreases more slowly than it does with the cavitation/aeration disabled, and the behaviour during the peak, when the compression stops and extension starts, has a different shape with a sharper edge. Still, the results indicate that, with the right values, the pressure behaviour should be close to the values calculated with the Peng-Robinson equation of state, which is regarded as being more accurate than the polytropic equation of state, (Equation 42).

There is a significant difference between the temperature behaviour in the two cases. Modelling the nitrogen and the hydraulic oil separately, simulates, in fact, a situation where a thin plate is placed between the two phases. This results in a high temperature, approximately 110 ºC, during compression and -20 ºC when the extension stops. For the purposes of this thesis, this unrealistic behaviour was acceptable, as the pressure behaviour was considered to be more important than the temperature behaviour. The conduction submodel transfers some heat from the gas to the hydraulic oil, but the heat transfer coefficient in the conduction submodel can not be set too high, as it will degrade the pressure behaviour in the orifice support. The reason for this is that the pressure inside the shock absorber is directly related to the force measured during compression, which can be clearly seen from Equation (27).

When cavitation/aeration is enabled, the temperature is almost a constant, with less than 1 ºC of variation during the static case simulation. This is as expected, as the nitrogen mixes with, or is in direct contact with, the hydraulic fluid. Even though the nitrogen temperature rises during compression, there are considerable differences between the thermal capacities and the masses of the nitrogen and the hydraulic fluid. In fact, there is no significant temperature rise in the orifice support during the simulation, which is close to reality. Indeed the landing measurements, used in the validation pro-

cess also revealed a temperature variation of 1 ℃. However, the exact location of the measurements is unknown, so the temperature rise during compression and the heat transfer between the two phases need a more detailed analysis.

Overall, enabling the cavitation/aeration option improves the temperature behaviour of the model but might make the pressure behaviour worse. A precise analysis of the variables in the cavitation/aeration calculations must be done in order to obtain the best possible results, during which the polytropic index can not be set as a constant. Such a change would, however, make the simulation of an underfilled shock absorber possible, which will be important in future research.

6.2   Other improvements

The piston submodels presented in this thesis are modelled as having rigid bodies, so even the high pressure chamber has no deformation during compression. This assumption of rigidity is well justified as far as the low pressure side is concerned, as on this side the pressure level only has a magnitude of tens of bars, rather than the hundreds of bars which are measured in the high pressure chamber. A hard landing with a high sink speed could generate pressure so high that the wall of the high pressure chamber would yield substantially. This would be manifested as a lower pressure inside the high pressure chamber than is manifested by the pressure of a rigid body, because the internal volume of the cylinder would increase. Even a small deformation might contribute to gas leakage out of the high pressure chamber, if the seals and the bearings also deform. Such a deformation could also cause a misalignment between the primary piston assembly and the orifice support.

Another improvement concerns the friction between the secondary piston assembly and the high pressure chamber. This friction is rather high in the simulations and a more detailed analysis should be made. This could actually be done by conducting a series of low frequency compression tests on the static test bench with different pressures inside the shock absorber. The deformation and the friction of the high pressure chamber could be solved with finite element analysis of a realistically modelled shock absorber. The way the metering pin and the orifice are modelled in this thesis is adequate for the objectives of this thesis, but a more detailed model is needed improve the accuracy of the damping behaviour of the shock absorber. In order to do this, the shape of the metering pin would first have to be measured very precisely. Secondly, other numerical methods, such as the finite volume method, should be used to solve the flow field over the orifice during compression. Finally, in order to make the model even more accurate, the results from the finite element and the finite volume analysis should also be incorporated.

The accuracy of the model could be further improved by measuring the amount of nitrogen that is inside a normally-serviced shock absorber. The shock absorber is filled until a certain pressure is reached, but its mass may vary depending on the temperature

of the nitrogen, and this can affect the pressure behaviour, as discussed in Chapter 5.2. Therefore, more precise information about the volume of the nitrogen is needed. Once these improvements have been made to the model, it should be incorporated into a multibody and multidimensional model. This model must be able to treat roll, pitch and yaw, which affect the impact loads, and it must also model the effects of gravity, lift force, thrust and sink speed on the landing gear. This would help in understanding the dynamics of the landing gear and its shock absorber, as well as the aircraft's overall behaviour during landing, this being the ultimate objective in modelling the main landing gear.

7.   CONCLUSIONS

The main objective of this thesis was to build a model which could produce realistic simulations of the behaviour of a modified oleo-pneumatic shock absorber, and the model presented in this thesis fulfils this objective. However, the model could be improved as it does not yet model all the physical phenomena which occur in operation. Nevertheless, even in its current state, the load-stroke behaviour of the model is close enough to reality for the model to be used to analyse the forces and pressures generated by different shocks as it shows close agreement with the reference measurement data used in the validation process.

Three different test cases were simulated during the validation process: a static test bench, a dynamic test and a real landing. The model performed well during each of these cases. The velocity in the dynamic test simulation did display some fluctuation when the second part of the stroke was reached and the high pressure side engages. This fluctuation was traced back to the mass envelope submodel which was used to model the two main parts of the shock absorber, i.e. the primary piston assembly and the high pressure chamber. However, changing the parameters of the mass envelope submodel leads to undesirable behaviour in the other two tests, so the fluctuations were tolerated because the other properties that were monitored were satisfactory.

The exact volume of nitrogen is difficult to calculate precisely, and even a small error can have a great impact on the behaviour of the model. Although the accuracy of the model was sufficient for our purposes, there remains some uncertainty about the volume and friction values. For example, exceptionally high friction values were observed during the validation procedure. Furthermore, the Karnopp friction model was used to model the friction and some of the stick-slip behaviours observed during the simulations were not present in the reference measurements, so clearly, more detailed measurements are needed.

The gas-liquid ratios were varied between the simulations, and it was observed that as the quantity of gas increases, the shock absorber loses some of its damping, which could lead to the landing gear malfunctioning during landing. The effect of temperature variation on the pressure behaviour inside the orifice support was also studied. This research showed it possible to simulate conditions under which the shock absorber is filled with fluids stored at the initial temperature conditions. The initial temperature affects the amount of nitrogen in the shock absorber, as cold conditions increase the density of the nitrogen, and therefore the mass inside the shock absorber. Therefore, filling the chambers with cold fluids increases the pressure. This implies that the shock ab-

sorber should always be filled with fluids at the ambient temperature, if possible. The temperature was also varied by heating or cooling the shock absorber once the simulation had been started. This was done to simulate the differences between the service and environmental conditions. It was noted that when the shock absorber is heated the pressure increases inside the orifice support and the high pressure chamber, and when it is cooled, the pressure decreases. This affects the overall displacement and velocity during compression. However, it is difficult to ascertain whether these differences in behaviour have any significant effect on the overall operation of the shock absorber.

The thesis discussed future improvements which could be made to the model. For example, putting the gas and the hydraulic fluid in the same volume presents a problem. The temperature of the gas within the orifice support is at unrealistic levels, and the absorption of the gas into the liquid has not been modelled. Foaming or cavitation can occur inside the shock absorber, and these phenomena are certainly areas for future study.
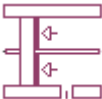
REFERENCES

[1]   Hoffren J., Saarela, O., Lentotekniikan perusteet, Edita Prima Oy, Helsinki, Finland, 2008, 199 p.

[2]   Dixon J., The Shock Absorber Handbook, John Wiley & Sons Ltd, Chichester, England, 2007, 415 p.

[3]   Hadekel, R., Shock Absorber Calculations, The Aircraft Engineering, Volume 19, Iss. 7, 1940, pp. 71-73.

[4]   Milwitzky B., Cook F., E., Analysis of Landing-gear Behavior, NACA Report 1154, Langley Field, USA,1953, 45 p.

[5]   Yadav, D., Ramamoorthy, R., P., Nonlinear Landing Gear Behaviour at Touchdown, Journal of Dynamic Systems, Measurement and Control, Volume 113, Iss. 4, 1991, pp. 677-683.

[6]   Daniels, J., N., A Method for Landing Gear Modeling and Simulation with Experimental Data, NASA Contractor Report 201601, Hampton, USA, 1996, 87 p.

[7]   Horta L., Daugherty R., Martinson V., Modeling and Validation of a Navy A6-Intruder Actively Controlled Landing Gear System, Technical Report, NASA Langley Research Center, Hampton, USA, 1999, 33 p.

[8]   Reineh M., Physical Modeling and Simulation Analysis of an Advanced Automotive Racing Shock Absorber Using the 1D Simulation Tool AMEsim, Master's thesis, Linköping, Sweden, 2012, 78 p.

[9]   Ljung, L., Glad, T., Modeling of Dynamic Systems, PTR Prentice Hall, New Jersey, USA, 1994, 361 p.

[10]   Currey, N., S., Aircraft Landing Gear Design: Principles and Practices, AIAA Inc., Marietta, USA, 1988, 363 p.

[11]   LMS Imagine.Lab AMEsim, Thermal Hydraulic Library Rev 13, User's guide, 2013, 79 p.

[12]   LMS Imagine.Lab AMEsim, Pneumatic Library Rev 13, User's guide, 2013, 89 p.

[13]   LMS Imagine.Lab AMEHelp, Online help file. 2010.

[14]   LMS Imagine.Lab AMEsim, Mechanical Library Rev 13, User's guide, 2013, 165 p.

[15]   Aaltonen J., Koskinen K., T., Hydraulic Cylinders, Encyclopedia of Tribology, Springer, New York, 2013, 4139 p.

[16]   Çengel Y., A., Boles, M., A., Thermodynamics: an Engineering Approach, 7th Edition, McGraw-Hill, New York, USA, 2011, 978 p.

[17]   Soave G., Equilibrium Constants From a Modified Redlich-Kwong Equation of State, Chemical Engineering Science, Vol. 27, 1972, pp. 1197-1203.

[18]   Redlich, O., Kwong, J., N., S., On the Thermodynamics of Solutions; an Equation of State; Fugacities of Gaseous Solutions, Symposioum on Thermodynamics and Molecular Structure of Solutions, Portland, USA, 1948.

[19]   Peng D., Y., Robinson D., B., A New Two-Constant Equation of State, 4th International Heat Transfer Conference, Paris-Versailles, France, 1970.

[20]   Hill T., L., An Introduction to Statistical Thermodynamics, Addison-Wesley Publishing Company inc., USA, 1960, 508 p.

[21]   LMS Imagine.Lab AMESim, Integration Algorithms used in AMESim, Technical bulletin 102, 2013, 11 p.

[22]   Petzold, L., Automatic Selection of Methods for Solving Stiff and Nonstiff Systems of Ordinary Differential Equations, SIAM Journal on Scientific and Statistical Computing, Vol 4, Iss. 1, 1983, pp. 136-148.

[23]   Griffiths, D., F., Higham, D., J., Numerical Methods for Ordinary Differential Equations: Initial Value Problems, Springer, New York, USA, 2010, 271 p.

[24]   Gear, W., C., Numerical Initial Value Problems in Ordinary Differential Equations, Prentice-Hall Inc., New Jersey, USA, 1971, 250 p.

[25]   Versteeg H., K., Malalasekera W., An Introduction to Computational Fluid Dynamics, 2nd Edition, Pearson Education Limited, England, 2007, 503 p.

[26]   Scheck, C., G., Thermal Hysteresis Loss in Gas Spring, Master's Thesis, Ohio, USA, 1988, 81 p.

[27]   LMS Imagine.Lab AMESim, HYD Advanced Fluid Properties, Technical bulletin 117, 2013, 27 p.

[28]   Conway, H., G., Landing gear design, Chapman & Hall, London, England, 1958, 342 p.

APPENDIX 1: AMESIM SUBMODEL SYMBOLS

SIGUDA01, reads a XY table and interpolates data as a function of time

PID001, a P.I.D. controller

GT00, makes a comparison between the inputs x and y and returns a signal of value 1 if x > y, 0 otherwise

FXA001, duty cycle submodel in which the output is defined by a function of an input

CONS00, outputs a signal with a constant specified value k

GA00, a simple gain

JUN3M, output is the difference between the input signals

PNRGD00, pneumatic real gas definition

PNPA002, pneumatic piston

PNCH012, pneumatic volume with temperature and pressure dynamics

PNCH013, pneumatic volume with temperature and pressure dynamics and heat exchange

THCD00, generic conduction model

THBC12, thermal-hydraulic volume with temperature and pressure dynamics and heat exchange

THBC11, thermal-hydraulic volume with temperature and pressure dynamics

THBAP12, thermal-hydraulic piston

THBAF02, leakage with variable length, eccentricity and viscous friction

DT00, a displacement transducer

MECVS0A, linear velocity sensor

FORC, converts a dimensionless signal input to a force with the same value

F000, zero force source

FR1T0010, a friction force generator with Coulomb and stiction friction

MAS001, 1 port mass capable of one-dimensional motion

MAS30, one-dimensional motion of a body within an envelope, friction and elastic end stops

GRAV0, sets the gravity of the system

TFPS00, thermal-hydraulic pressure sensor

TFVR1, variable thermal-hydraulic restriction

TFFD3, thermal-hydraulic advanced properties with cavitation